Table 2. Protein expression profiles of $CD34^+/CD38^-$ and $CD34^+/CD38^+$ AML cells

NCBI accession no.	Protein	Average iTRAQ ration (114/115)	Average iTRAQ ration (116/117)	Gene symbol
P27701	Adhesion: CD82 antigen	4.64	3.79	CD82 (KAI1)
Q9H165	Apoptosis: Isoform 1 of B-cell lymphoma/leukemia 11A	5.79	6.38	BCL11A (CTIP1)
P47738	Enzyme: Aldehyde dehydrogenase, mitochondrial precursor	5.22	4.43	ALDH
Q9H0C8	Enzyme: Integrin-linked kinase-associated serine/threonine phosphatase 2C	4.29	10.52	ILKAP
P01903	Immunity: HLA class II *histocompatibility* antigen, DR alpha chain precursor	6.11	3.87	HLA-DRA

labeled with a specific isobaric iTRAQ reagent. To compensate for extreme sample complexity, each iTRAQ sample was separated into 24 fractions using strong cation-exchange chromatography.[23] A total of 2,537 and 2,506 proteins were identified with >95% confidence for each of the biological replicates. Since iTRAQ internal replicates typically yield high confidence results,[27] differences greater than threefold or less than 0.5-fold are considered significant. We listed the proteins whose expression was greater than 3-fold or less than 0.5-fold in $CD34^+/CD38^-$ AML cells as compared with their $CD34^+/CD38^+$ counterparts in Table 2 and Supporting Information Table 2. Either 481 or 700 proteins were differentially expressed in case 1 and case 2, respectively (Table not shown), and only 104 proteins were overlapped in both cases (Table 2, Supporting Information Table S1).The expression of 98 of these proteins increased, while the expression of six proteins decreased in both cases (Table 2, Supporting Information Table S1). Two of the identified proteins are involved in differentiation, two play a role in the cell cycle, six play a role in adhesion, five are involved in DNA replication and repair, and eight are involved in apoptosis and anti-apoptosis (Table 2, Supporting Information Table S1). In addition, 6 nuclear transcription factors, 17 enzymes involved in drug-resistance, 6 human leukocyte antigens, 18 ribosome nucleoproteins, and 10 histone and histone-binding proteins were differentially expressed between $CD34^+/CD38^-$ AML and $CD34^+/CD38^+$ counterparts (Supporting Information Table S1). Additional differentially expressed proteins are also listed in Supporting Information Table S1. Other studies identified aldehyde dehydrogenase activity (ALDH), B-cell lymphoma/leukemia 11A (BCL11A), ILK, and HLA-DR as highly expressed proteins in leukemia stem cells.[28–31] These proteins were also overexpressed in $CD34^+/CD38^-$ AML cells in the present study (Table 2), indicating an acceptable sensitivity of the current study.

CD82 is overexpressed in $CD34^+/CD38^-$ AML cells

We focused on CD82 because this protein functions as an adhesion molecule that is important to maintain the character of LSCs. We attempted to validate these results in other $CD34^+/CD38^-$ AML cells isolated from patients (11 from BM, 5 from PB, cases 1–14, 17, 18) by FACS. In 15 of 16 cases (94%), the relative expression levels of CD82 were significantly higher in $CD34^+/CD38^-$ AML cells (68 ± 27%) as compared with their $CD34^+/CD38^+$ counterparts (30 ± 19%) ($p < 0.01$, Fig.1*a*, Supporting Information Fig. S2*a*). On the other hand, a mean 35 ± 19% of $CD34^+$ hematopoietic stem/progenitor cells isolated from healthy volunteers ($n = 6$) were positive for CD82 staining (Supporting Information Fig. S2*b*). In addition, we found that imatinib-resistant EOL-1R cells which stayed on a dormant state and possessed the immature character with aberrant expression of CD34 (data not shown) expressed a greater amount of CD82 on their cell surface (96 ± 1%) than parental EOL-1 cells (47 ± 4%) (Fig. 1*a*).

The MMPs enzymatic activity

Aberrant expression of CD82 was associated with inactivation of matrix metalloproteinase 9 (MMP9) in the H1299 human lung carcinoma cells.[14] We therefore examined the relationship between CD82 and MMPs in $CD34^+/CD38^-$ AML cells. Real-time RT-PCR found that the levels of MMP9 were significantly lower in CD82 over-expressed $CD34^+/CD38^-$ AML cells than their $CD34^+/CD38^+$ counterparts ($n = 7$, $p < 0.01$) (Fig. 1*b*). On the other hand, levels of MMP2 in $CD34^+/CD38^-$ AML cells were almost identical to those in $CD34^+/CD38^+$ counterparts (Fig. 1*b*). We also found that the levels of both MMP-9 and -2 were down-regulated in imatinib-resistant EOL-1R cells as compared with parental EOL-1 cells (Fig. 1*b*). To explore a potential link between CD82 and MMPs in leukemia cells, EOL-1R cells were transiently transfected with either scrambled control or CD82 siRNA (Fig. 1*c*), which efficiently decreased levels of CD82 in these cells (from 96 ± 1% to 41 ± 1%, Fig. 1*c*). The MMPs enzymatic activity in these cells was determined by performing gelatin zymography with the culture supernatant as well as whole cell proteins extracted from EOL-1 and EOL-1R cells (Fig. 1*d*). Interestingly, when CD82 was down-regulated in EOL-1R cells by an siRNA, enzymatic activity of MMP9 was dramatically increased (Fig. 1*d*), suggesting that CD82 negatively regulated MMP9. Real-time RT-PCR found that

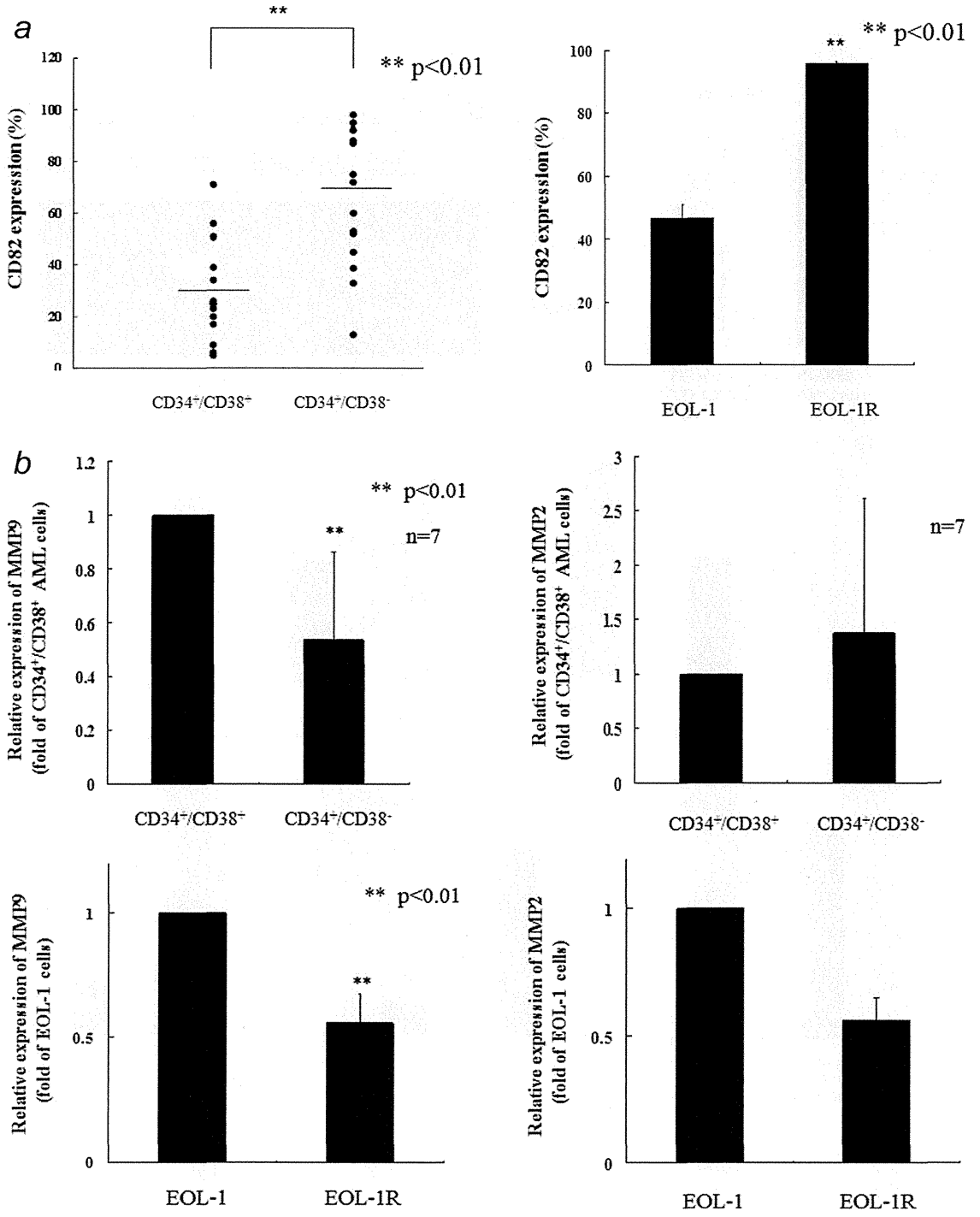

Figure 1. CD82 expression in $CD34^+/CD38^-$ AML cells and $CD34^+/CD38^+$ counterparts. (*a*) Leukemia cells isolated from patients (BM, $n = 11$; PB, $n = 5$) were stained with anti-CD34, -CD38, and -CD82 antibodies. Expression of CD82 in $CD34^+/CD38^-$ AML cells and their $CD34^+/CD38^+$ counterparts was analyzed using FlowJo. Each dot represents expression of CD82 for an individual and the mean value is indicated by the line. EOL-1 or EOL-1R cells were stained with anti-CD82 antibody. Expression of CD82 in EOL-1 or EOL-1R cells was analyzed using FlowJo. Statistical significance was determined by paired *t*-test. $^{**}p < 0.01$, with respect to control. The effect of CD82 on MMPs. Real-time RT-PCR. (*b*) RNA was extracted from EOL-1, EOL-1R, and $CD34^+/CD38^-$ cells and their $CD34^+/CD38^+$ counterparts isolated from AML patients. cDNAs were synthesized and subjected to real-time RT-PCR to measure the levels of MMP9 and MMP2. Results represent the mean ± SD of three experiments performed in triplicate. The statistical significance was assessed by a paired *t*-test. $^{**}p < 0.01$;$^{*}p < 0.05$. FACS. (*c*) EOL-1 cells were transiently transfected with either scrambled control or CD82 siRNA. After 24 hr, cells were subjected to FACS to quantity the proportion of CD82-expressing cells. Gelatin zymography. (*d*) EOL-1 and EOL-1R cells were transfected with either scrambled control or CD82 siRNA. After 48 hr, whole cell lysates and culture supernatant were collected. The enzymatic activity of MMPs was determined by a gelatin-zymography kit, following the manufacturer's instructions. Real-time RT-PCR. (*e*) EOL-1R cells were transfected with either scrambled control or CD82 siRNA. After 24 hr, these cells were collected and mRNAs were extracted. cDNAs were synthesized and subjected to real-time RT-PCR to measure the levels of MMP9 and MMP2. Results represent mean ± SD of duplicate cultures. $^{**}p < 0.01$; $^{*}p < 0.05$. FACS. (*f*) $CD34^+/CD38^-$ AML cells (cases 1, 2, 6, and 14) were transduced with either control or CD82 shRNA. (*h*) $CD34^+/CD38^+$ AML cells (cases 1, 2, 14, and 15) were transduced with either empty vector or CD82-expressing lentiviral particles. These cells were subjected to FACS to quantity the proportion of CD82-expressing cells. Real-time RT-PCR. (*g*) $CD34^+/CD38^-$ (cases 1, 2, and 6) or (i) $CD34^+/CD38^+$ AML cells (cases 1, 2, 14, and 15) transduced with CD82 shRNA or CD82-expressing lentiviral particles were collected and mRNAs were extracted. cDNAs were synthesized and subjected to real-time RT-PCR to measure the levels of MMP9. Each dot represents the levels of MMP9 for an individual experiment and the mean is indicated by the line. $^{**}p < 0.01$; $^{*}p < 0.05$.

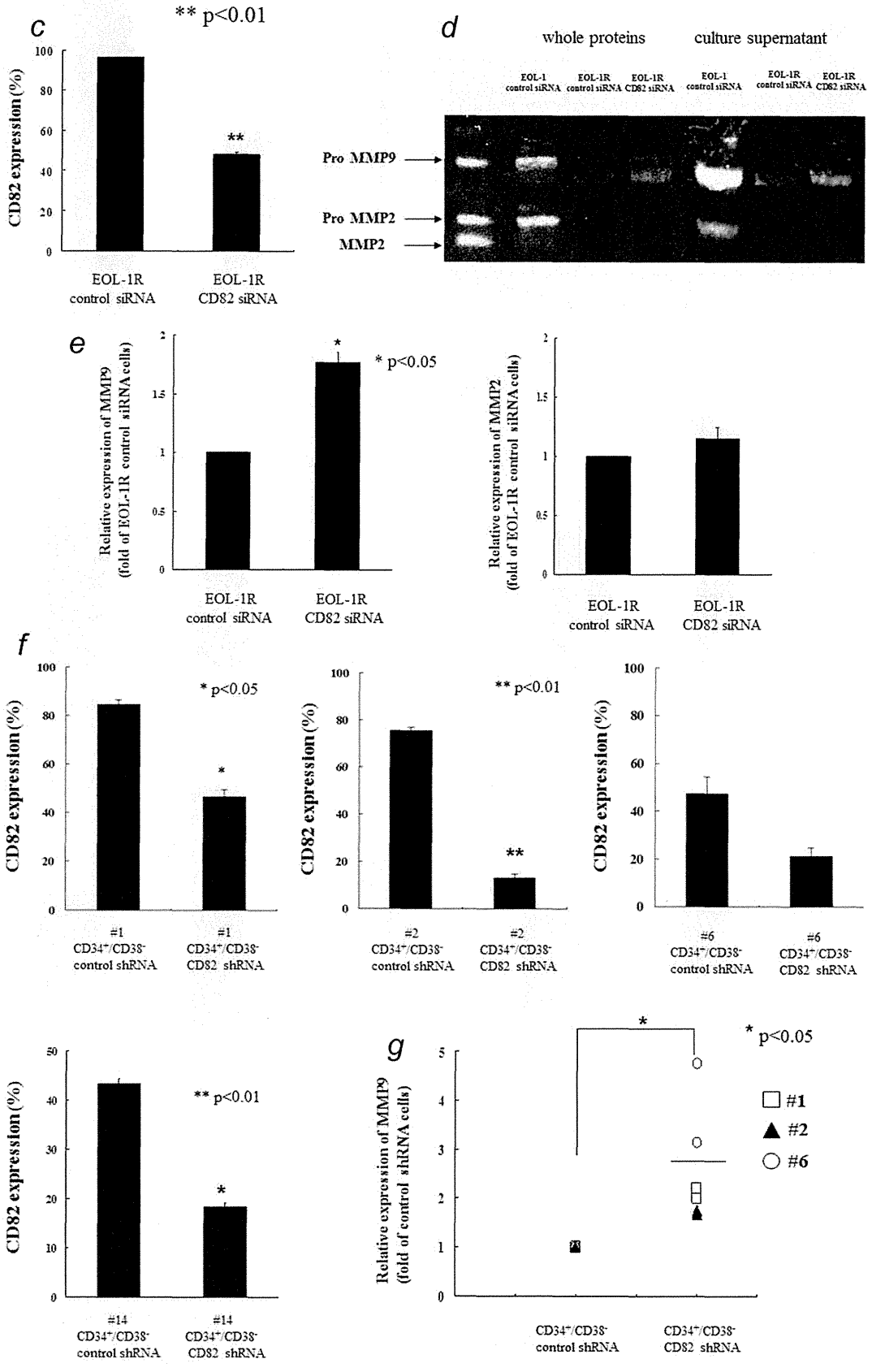

Figure 1. (Continued)

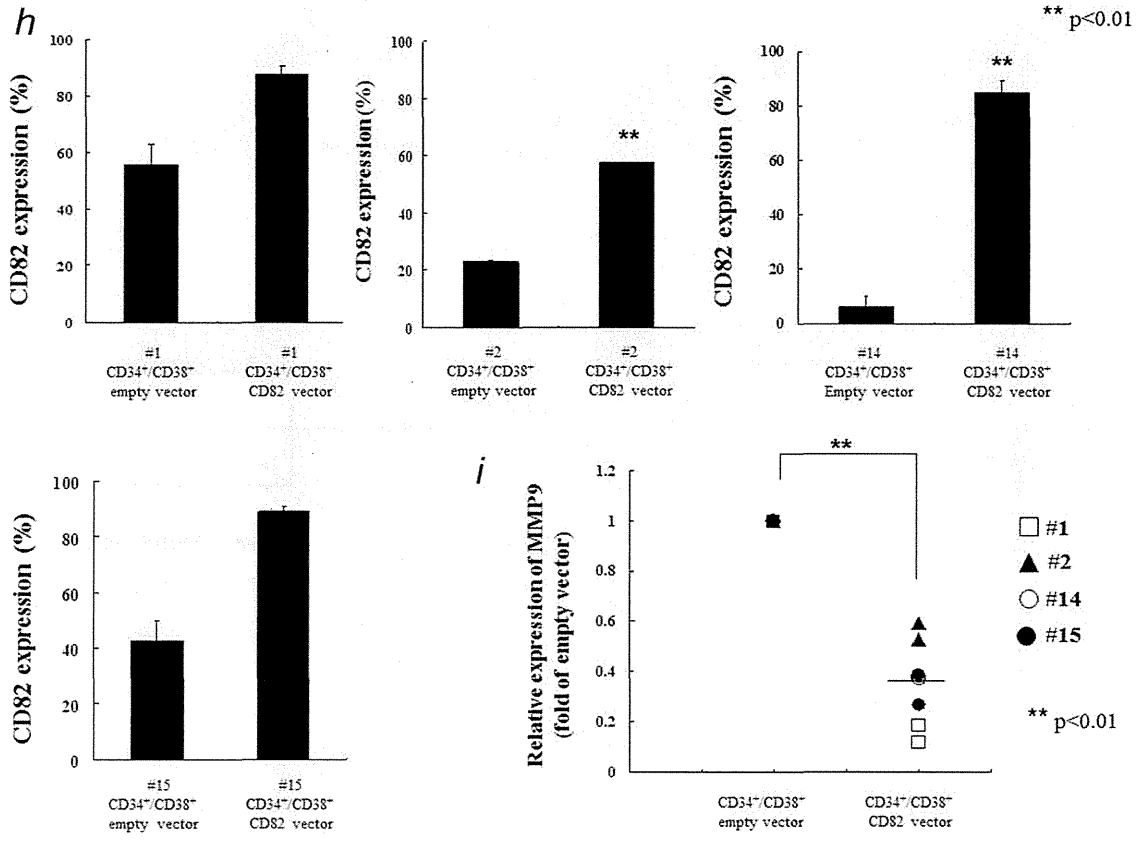

Figure 1. (Continued)

down-regulation of CD82 by an siRNA increased levels of MMP9 by nearly twofold in EOL-1R cells (Fig. 1*e*). On the other hand, levels of MMP2 were not affected by down-regulation of CD82 (Fig. 1*e*). Moreover, to explore the function of CD82 in freshly isolated $CD34^+/CD38^-$ AML cells, we genetically down-regulated CD82 in these cells. An shRNA targeting CD82 decreased expression of CD82 in four cells (case 1, from 85 ± 2% to 47 ± 3%; case 2, from 75 ± 1% to 13 ± 2%; case 6, from 47 ± 7% to 21 ± 3%, $p = 0.066$; case 14, from 43 ± 1% to 18 ± 1%, Fig. 1*f*). Real-time RT-PCR found that the levels of MMP9 were significantly increased after down-regulation of CD82 in $CD34^+/CD38^-$ AML cells ($n = 3$, cases 1, 2, and 6, $p < 0.05$, Fig. 1*g*). We next exposed $CD34^+/CD38^+$ AML cells to the CD82-expressing lentiviral particles, which increased levels of CD82 ($n = 4$, case 1; from 56 ± 7% to 88 ± 3%, case 2, from 23 ± 1% to 58 ± 1%; case 14; from 6 ± 4% to 85 ± 4%, case 15; from 43 ± 7% to 89 ± 2%, Fig. 1*h*). As expected, the levels of MMP9 were decreased by half in these cells (Fig. 1*i*).

The effects of CD82 on migration of $CD34^+/CD38^-$ AML cells

We next examined the function of CD82 in $CD34^+/CD38^-$ AML cells. When levels of CD82 were down-regulated in $CD34^+/CD38^-$ AML cells after lentiviral transduction of CD82 shRNA ($n = 4$. cases 1, 2, 6 and 14, Fig. 1*f*), their migration was significantly stimulated (Fig. 2*a*). Moreover, we enhanced expression of CD82 in $CD34^+/CD38^+$ AML cells by using CD82-expressing lentiviral particles ($n = 3$, cases 1, 14 and 15, Fig. 1*h*). Forced-expression of CD82 in $CD34^+/CD38^+$ AML cells dramatically increased number of cells adhered to the insert in parallel with a decrease in the number of migrated cells (Fig. 2*b*). Similarly, after down-regulation of CD82 in EOL-1R cells, adhesive cells decreased by approximately half (Fig. 2*c*). In parallel, population of EOL-1R cells migrated to the lower well increased by 10-fold after down-regulation of CD82 in these cells (Fig. 2*c*).

The effect of CD82 on colony forming ability of $CD34^+/CD38^-$ AML cells

We first examined whether CD82 regulated proliferation of $CD34^+/CD38^-$ AML cells (cases 1, 6, and 14) by using colony forming assay (Fig. 3*a*). Down-regulation of CD82 by an shRNA (from 59 to 27%) inhibited their colony forming ability by approximately 50% (Fig. 3*a*). Likewise, down-regulation of CD82 by an siRNA (from 96% to 48%) inhibited colony forming ability of $CD34^+$ EOL-1R cells which mimic LSCs by mean 50% (Fig. 3*b*). On the other hand, forced-expression of CD82 in $CD34^+/CD38^+$ AML cells (cases 1 and 14) by transduction of CD82-expressing lentiviral particles increased levels of CD82 from 18 to 89% and stimulated their colony forming ability by mean 1.7-fold (Fig. 3*c*).

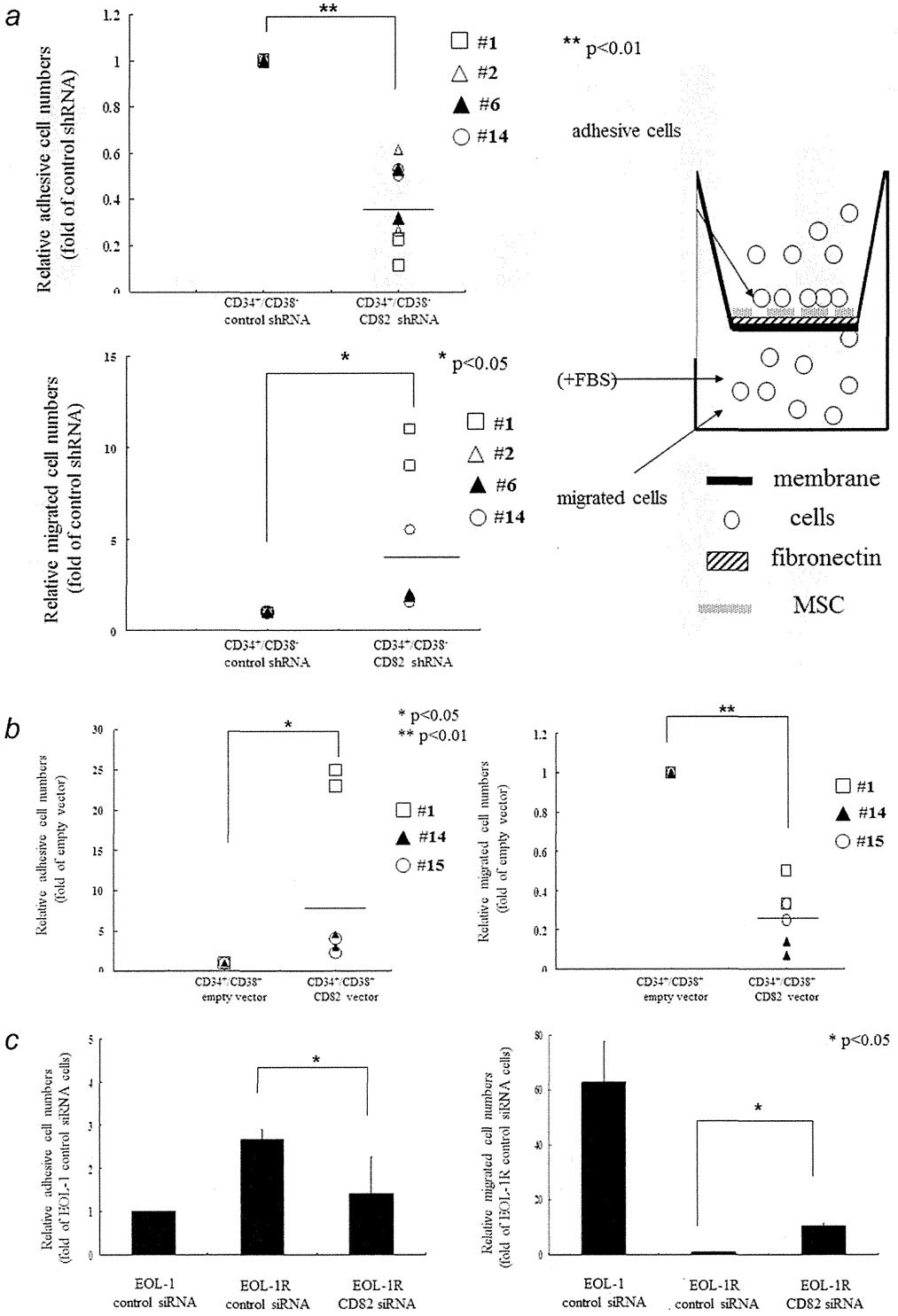

Figure 2. The effects of CD82 on migration of leukemia cells. Migration assays. (*a*) $CD34^+/CD38^-$ (cases 1, 2, 6, and 14) or (*b*) $CD34^+/CD38^+$ AML cells (cases 1, 14, and 15) transduced with CD82 shRNA or CD82-expressing lentiviral particle were seeded in the upper biocoat cell culture inserts. After 48 hr, the cells that had migrated through the filters were stained with 4'6-diamidino-2-phenylindole, and counted under a microscope. Each dot represents relative adhesion or migration cell numbers for an individual experiment and the mean is indicated by the line. (*c*) EOL-1 and EOL-1R cells transfected by either scrambled control or CD82 siRNA were seeded in the upper biocoat cell culture inserts. After 48 hr, the cells that had migrated through the filters were stained with 4'6-diamidino-2-phenylindole, and counted under a microscope. Results represent the mean ± SD of two experiments performed in triplicate cultures. $^{**}p < 0.01$; $^{*}p < 0.05$.

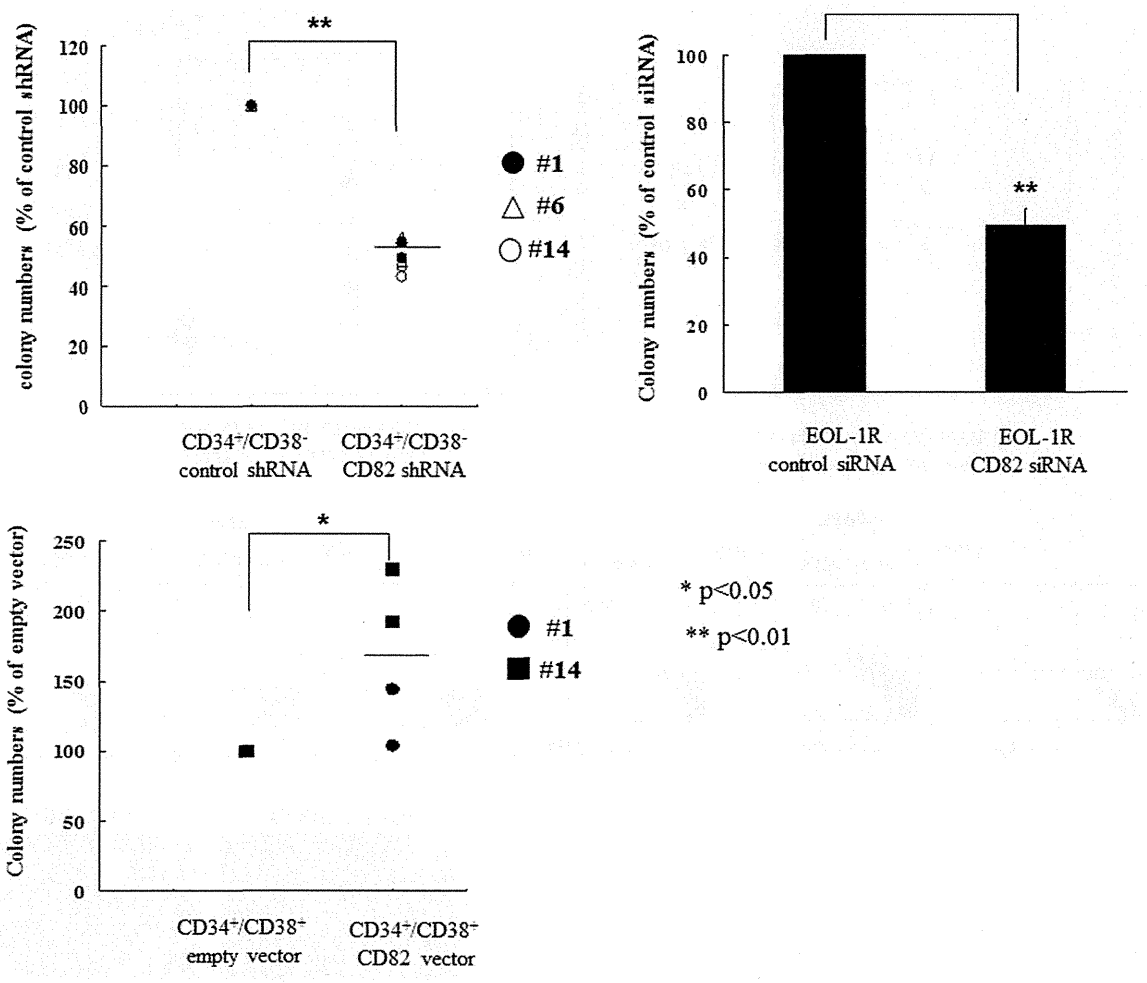

Figure 3. The effect of CD82 on proliferation of $CD34^+/CD38^-$ AML cells. Colony forming assay. (*a*) $CD34^+/CD38^-$ (cases 1, 6, and 14) or (*c*) $CD34^+/CD38^+$ AML cells (cases 1 and 14) were transduced with CD82 shRNA or CD82-expressing lentiviral particles. (*b*) EOL-1R cells were transiently transfected with either control or CD82 siRNA. These cells were cultured in methylcellulose medium. After 16 days, colonies were counted. Each dot represents % of colony number compared with control for an individual experiment and the mean is indicated by the line.

These observations suggested that CD82 plays a role in survival of $CD34^+/CD38^-$ AML cells.

AML engraftment was inhibited by down-regulation of CD82 *in vivo*

We next examined the function of CD82 *in vivo*. $CD34^+/CD38^-$ cells isolated from three different AML patients (cases 1, 6 and 14) were transduced with either scrambled control or CD82 shRNA. We transplanted these cells into NOD.Cg-*Rag1*^{tm1Mom} *Il2rg*^{tm1Wjl}/SzJ mice *via* the tail vein. Transplanted mice were sacrificed at 9 weeks after transplantation and analyzed the human engraftment in their spleens and BM by quantifying the population of positive cells for human CD45 and CD33 antigens (Figs. 4*a* and 4*b*). Transplantation of $CD34^+/CD38^-$ AML cells transduced by scrambled control shRNA resulted in the mean human engraftment either 14 ± 6% or 15 ± 5% in spleen and BM, respectively ($n = 8$, Fig. 4*a*). These cells expressed CD33antigen on their cell surface (4% in both spleen and BM) (Fig. 4*b*). On the other hand, when these cells were transduced with CD82 shRNA, human engraftment was significantly impaired (7 ± 4% or 6 ± 2% in spleen and BM, respectively, $p < 0.01$) ($n = 6$, Fig. 4*a*). In addition, population of cells expressing CD33 on their cell surface was decreased to either 0.1% or 1% in spleen and BM, respectively (Fig. 4*b*). These observations suggested that down-regulation of CD82 impaired AML engraftment as well as AML reconstitution in an immunodeficient mice. In addition, we assessed levels of CD82 and MMP9 in isolated $CD34^+/CD38^-$ AML cells ($n = 9$) by using single cell real-time RT-PCR (Fig. 4*c*). Inverse correlation was noted between levels of CD82 and MMP9 ($r = -0.58$, Fig. 4*c*). Moreover, we examined the levels of CD82 in transplanted human AML cells as well as localization of these cells in murine BM by immunohistochemistry (Figs. 4*d*–4*g*). Notably, human AML cells expressing CD82 were localized in endosteal region of BM at 9 weeks after

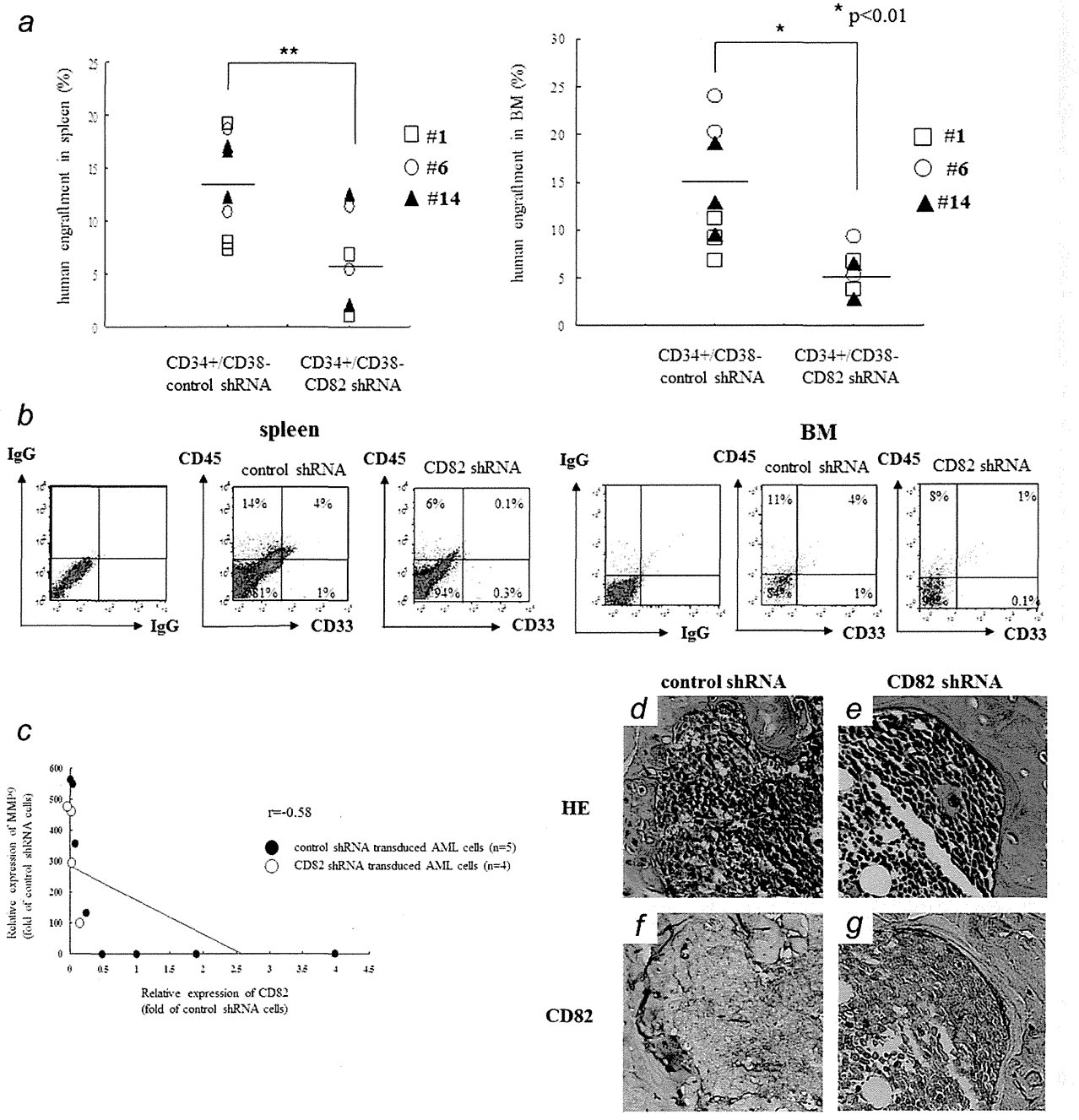

Figure 4. Down-regulation of CD82 impairs the AML engraftment. $CD34^+/CD38^-$ AML cells were isolated from three AML patients (cases 1, 6, and 14) and transduced with either scrambled control or CD82 shRNA. These cells were transplanted into NOD.Cg-*Rag1*^{tm1Mom} *Il2rg*^{tm1Wjl}/SzJ mice *via* the tail vein. At 9 weeks after transplantation, mice were euthanized and then spleen were removed. AML engraftment. (*a*) The percentages of human CD45 were analyzed to monitor the human engraftment in murine spleen and BM (scrambled control shRNA; $n = 8$, CD82 shRNA; $n = 6$) by using flow cytometry. Each dot represents CD45 expression for an individual experiment and the mean is indicated by the line. FACS. (*b*) Spleen and BM cells isolated from NOD.Cg-*Rag1*^{tm1Mom} *Il2rg*^{tm1Wjl}/SzJ mice received transplantation of $CD34^+/CD38^-$ AML cells (cases 1, 6, and 14) transduced with either CD82 shRNA or control shRNA were stained with anti-human CD45 and CD33 antibodies. Representative flow cytometric analyses of human CD45 and CD33 expression in murine spleen and BM cells are shown. Relationship between MMP9 and CD82. (*c*) A single $CD34^+/CD38^-$ AML cell was isolated from murine BMs by BD FACS AriaII. These cells were subjected to reverse transcription by AmpliSpeed slide cycler and the synthesized cDNA was subjected to real-time PCR to measure the levels of CD82 and MMP9. Results showed relative expression of MMP9 *versus* that of CD82. For demonstration of association, the Pearson's correlation coefficient test was applied. ●Scrambled control shRNA; $n = 5$, ○CD82 shRNA; $n = 4$. Immunohistochemistry. BMs were removed from mice, who were transplanted with either (*d*, *f*) scrambled control or (*e*, *g*) CD82 shRNA transduced $CD34^+/CD38^-$ AML cells. These BMs were stained with either (*d*, *e*) hematoxylin and eosin (HE) or (*f*, *g*) an anti-human CD82 antibody (CD82) and examined under light microscope.

transplantation of scrambled control shRNA transduced $CD34^+/CD38^-$ AML cells (Figs. 4*d* and 4*f*). On the other hand, human AML cells were not detectable in this region of murine BM, that were transplanted with CD82-depleted $CD34^+/CD38^-$ AML cells (Figs. 4*e* and 4*g*). To examine longer-term reconstituting capability, we carried out secondary transplantation of $CD34^+/CD38^-$ AML cells recovered from primary recipient mice. At 9 weeks post-transplantation, human AML engraftment was 18% as assessed by quantification of human CD45 expressing cells in PB isolated from the secondary recipients by FACS. These observations suggested that functional properties of $CD34^+/CD38^-$ AML cells were maintained in the BM microenvironment of recipient mice and $CD34^+/CD38^-$ AML cells utilized in this study fulfill the criteria for LSCs *in vivo*.

Moreover, we examined whether CD82 affected homing of AML cells to BM. AML cells isolated from three patients (cases 6, 14, 17) were treated with anti-CD82 or control IgG antibody. These cells were transplanted per mouse, and homing of the cells was analyzed in the BM of mice after 16 hr of transplantation. In the control group ($n = 6$), an average of 0.39% in human $CD34^+$ AML cells were detected in the mouse BM compared with 0.77% in the CD82 antibody-treated group (Supporting Information Fig. S6).

Discussion

Previous studies showed that the LSCs-niche interaction was important to maintain the stemness of leukemia cells.[15] In this study, iTRAQ technique identified adhesion molecule CD82 as an overexpressed protein in $CD34^+/CD38^-$ AML cells (Supporting Information Table S1). Additional experiments utilizing FACS confirmed aberrant expression of CD82 in freshly isolated $CD34^+/CD38^-$ AML cells ($n = 16$) (Fig. 1*a*). In addition, this study found that down-regulation of CD82 by an shRNA increased levels of MMP9 in $CD34^+/CD38^-$ AML cells (Fig. 1*g*) and stimulated their migration (Fig. 2*a*). Meanwhile, forced expression of CD82 decreased levels of MMP9 mRNA in $CD34^+/CD38^+$ AML cells (Fig. 1*i*) and enhanced adhesion of these cells to fibronectin and MSCs, a kind of artificial BM niche (Fig. 2*b*). Single cell RT-PCR also demonstrated that down-regulation of CD82 by an shRNA increased levels of MMP9 mRNA in $CD34^+/CD38^-$ AML cells, and reverse correlation was noted between levels of MMP9 and CD82 in $CD34^+/CD38^-$ AML cells (Fig. 4*c*). The levels of MMP9 mRNA in $CD34^+/CD38^-$ AML cells shown in Figures 1*g* and 4*c* were inconsistent, although the cells utilized in these studies were isolated from same populations. In these studies shown in Figure 4*c*, we used a single cell immediately after isolation from murine BM. On the other hand, cells used in these studies shown in Figure 1*g* were incubated for 7 days in full media to be transduced by shRNA. As a result, the levels of MMP9 mRNA in leukemia cells might be down-regulated in these cells. Notably, down-regulation of CD82 in $CD34^+/CD38^-$ AML cells ($n = 3$) by an shRNA impaired engraftment of these cells in the BM as well as spleen in NOD.Cg-*Rag1*^{tm1Mom} *Il2rg*^{tm1Wjl}/SzJ mice (Fig. 4*a*). These observations suggested that CD82 played an important role in adhesion of $CD34^+/CD38^-$ AML cells to BM microenvironment *via* down-regulation of MMP9. Other investigators showed that MMP9 in human mononuclear phagocytes was inhibited by IL-10.[32] Similarly, IL-10 activated the tissue inhibitors of expression of metalloproteinases (TIMP-1/2) and down-regulated the levels of MMP2 and MMP9 in human prostate cancer cells.[33] Thus, down-regulation of MMP9 by IL-10 may augment adhesion of HSCs to BM osteoblastic niche and exogenous administration of IL-10 may be useful to promote the repopulating ability of HSCs and engraftment of HSCs to BM niche. We also found that exposure of $CD34^+/CD38^-$ AML cells to IL-10 (5 ng/ml) down-regulated levels of MMP9 mRNA in these cells (Supporting Information Fig. S5). On the other hand, down-regulation of IL-10 in these cells ($n = 2$, cases 2 and 6) by an shRNA increased levels of MMP9 by twofold (Supporting Information Fig. S5). Further experiments found that down-regulation of CD82 in $CD34^+/CD38^-$ AML cells by an shRNA potently down-regulated levels of IL-10 (in preparation for publication). Notably, forced expression of CD82 down-regulated levels of MMP9 mRNA, resulting in inactivation of MMP9 in leukemia cells (Figs. 1*d* and 1*e*). We therefore hypothesize that CD82 may inactivate MMP9 *via* IL-10 signaling in LSCs. MMP9 promotes mobilization of HSCs from the BM osteoblastic niche by release of soluble Kit-ligand (sKitL),[34] which increases the motility of HSCs and progenitors within the BM. In addition, MMPs cleave integrin β4 and β1 in cultured human corneal epithelial cells and mouse epidermal keratinocytes.[35] CD82 associates with various integrins including α3β1, α4β1 and α6β1.[36,37] Amongst them integrin α4β1 (VLA4) plays an important role in adhesion of LSCs to BM microenvironment.[38] We found that $CD34^+/CD38^-$ AML cells expressed a greater amount of integrin α4β1 (VLA4) than their counterparts, as measured by real time RT-PCR ($n = 5$, Supporting Information Fig. S7*a*). The hematopoietic cells adhere to stromal endothelial cells through the VLA4/vascular cellular adhesion molecule-1 (VCAM-1) pathway.[39] Thus, activation of MMP9 by down-regulation of CD82 may be able to mobilize $CD34^+/CD38^-$ AML cells from BM *via* disruption of interaction between VLA4 and VCAM-1 on cell surface of stromal cells. Moreover, to assess if CD82 interacts with VLA4 molecules, we utilized an anti-integrin β1 (CD29) Ab (Beckman coulter, CA, 6603113) which blocks adhesion of leukemia cells to fibronectine. Forced-expression of CD82 stimulated an adhesion of $CD34^+/CD38^+$ AML cells (case 15) to the artificial niche, which was hampered when these cells were treated with an anti-integrin β1 Ab (Supporting Information Fig. S7*b*). Furthermore, we examined interaction between CD82 and integrin α4 by utilizing Immunoprecipitation assay and found that CD82 directly interacted with integrin α4 (Supporting Information Fig. S7*c*). These observations suggested that VLA4 interacted with CD82 and played a role in adhesion of these cells to the artificial niche.

We found that blockade of CD82 on cell surface of AML cells by an antibody stimulated BM homing of $CD34^+$ AML cells in these mice (Supporting Information Fig. S6). Similar to the present study, other investigates also showed that cord blood (CB) $CD34^+$ cells treated with stem cell factor enhanced expression of MMP2/MMP9 and increased BM homing of human CB $CD34^+$ cells in NOD/SCID mice.[40,41] Thus, blockade of CD82 may increase levels of MMP9, resulting in enhanced migration of AML cells into the BM. However, we hypothesize that these cells could not fully adhere to the BM microenvironment and survive to develop AML.

Interestingly, the CXCR4 antagonist AMD3100 effectively mobilized AML cells without inducing their proliferation.[42] Preclinical studies showed that treatment of leukemic mice with a chemotherapeutic agent in combination with AMD3100 resulted in decreased tumor burden and improved their overall survival compared with mice treated with a chemotherapeutic agent alone. These observations provided a proof-of-principle for directing therapy to the critical tethers that promote AML-niche interactions[42] and supported our hypothesis that inhibition of CD82 could mobilize LSCs from BM niche and sensitize these cells to chemotherapeutic agents. Further studies are clearly required to test our hypothesis *in vivo*.

Another idea to sensitize LSCs to chemotherapeutic agents related to stimulation of cell-cycling of dormant LSCs. Recent studies showed that $CD34^+/CD38^-$ AML cells were induced to enter the cell cycle by treatment with G-CSF *in vivo*. G-CSF significantly enhanced apoptosis of $CD34^+/CD38^-$ AML cells mediated by cell cycle-dependent chemotherapeutic agents and eliminated $CD34^+/CD38^-$ AML cells from mice.[43] The additional experiments found that down-regulation of CD82 was not able to stimulate cell cycling of $CD34^+/CD38^-$ AML cells (cases 1 and 6) and EOL-1R cells (Supporting Information Fig. S3), suggesting that CD82 was not involved in the maintenance of dormancy in these cells.

CD82 inhibited the receptor tyrosine kinase human mesenchymal-epithelial transition factor (c-Met) activity,[44] which promoted proliferation and migration of cancer cells.[45,46] c-Met was shown to mediate G-CSF-induced mobilization of hematopoietic progenitor cells (HPCs) *via* reactive oxygen species (ROS) signaling.[47] Aberrant expression of CD82 in $CD34^+/CD38^-$ AML cells may inactivate c-Met and cause engraftment of these cells to BM niche. We found that levels of CD82 in $CD34^+$ hematopoietic stem/progenitor cells isolated from healthy volunteers ($n = 6$) were lower than those in $CD34^+/CD38^-$ AML cells (35% *vs.* 59%, $p = 0.02$, Supporting Information Fig. S4). Importantly, down-regulation of CD82 in $CD34^+$ hematopoietic stem/progenitor cells by an shRNA did not significantly inhibit their colony forming ability (Supporting Information Fig. S4).

CD82 expression was strongly correlated with the tumor suppressor gene p53.[48] On the other hand, other studies showed that levels of CD82 did not correlate with the expression of p53 in human hepatocellular carcinoma.[49] We also examined the correlation between CD82 and p53 mRNA levels in $CD34^+/CD38^-$ AML cells ($n = 6$) and their $CD34^+/CD38^-$ counterparts by utilizing real-time RT-PCR and found that the correlation coefficient was 0.54 (figure not shown). Thus, we think that expression of CD82 is not related with p53 in $CD34^+/CD38^-$ AML cells.

Overexpressed CD82 in AML cells may render these cells to adhere to BM niche and regulate maintenance of leukemia stem cells within BM niche. On the other hand, down-regulation of CD82 in AML cells may stimulate circulating of these cells from BM niche to PB.

Taken together, our data suggested that CD82 negatively regulated MMP9 and played an important role in $CD34^+/CD38^-$ AML cells to adhere to BM microenvironment. In addition, CD82 was involved in survival of $CD34^+/CD38^-$ AML cells. CD82 might be an attractive molecular target to eradicate LSCs in AML patients. Further studies are warranted to evaluate the function of CD82 in LSCs *in vivo*.

Acknowledgements

This work was supported in part by The Kochi University President's Discretionary Grant (to T.I.), Setsuro Fujii Memorial, The Osaka Foundation for Promotion of Fundamental Medical Research (to T.I.) and Certificate of Kochi Shin-kin/Anshin-tomo-no-kai Prize (to C.N.). C.N. is grateful for a JSPS Research Fellowship for Young Scientists from the Japan Society for the Promotion of Science.

References

1. Bonnet D, Dick JE. Human acute myeloid leukemia is organized as a hierarchy that originates from a primitive hematopoietic cell. *Nat Med* 1997;3:730–7.
2. Lapidot T, Sirard C, Vormoor J, et al. A cell initiating human acute myeloid leukaemia after transplantation into SCID mice. *Nature* 1994;367:645–8.
3. Blair A, Sutherland HJ. Primitive acute myeloid leukemia cells with long-term proliferative ability in vitro and in vivo lack surface expression of c-kit (CD117). *Exp Hematol* 2000;28:660–71.
4. Blair A, Hogge DE, Sutherland HJ. Most acute myeloid leukemia progenitor cells with long-term proliferative ability in vitro and in vivo have the phenotype CD34(+)/CD71(-)/HLA-DR-. *Blood* 1998;92:4325–35.
5. Clarke MF, Dick JE, Dirks PB, et al. Cancer stem cells-perspectives on current status and future directions: AACR Workshop on cancer stem cells. *Cancer Res* 2006;66:9339–44.
6. Ishikawa F, Yoshida S, Saito Y, et al. Chemotherapy-resistant human AML stem cells home to and engraft within the bone-marrow endosteal region. *Nat Biotechnol* 2007;25:1315–21.
7. Taussig DC, Miraki-Moud F, Anjos-Afonso F, et al. Anti-CD38 antibody-mediated clearance of human repopulating cells masks the heterogeneity of leukemia-initiating cells. *Blood* 2008;112:568–75.
8. Sarry JE, Murphy K, Perry R, et al. Human acute myelogenous leukemia stem cells are rare and heterogeneous when assayed in NOD/SCID/IL2Rγc-deficient mice. *J Clin Invest* 2011;121:384–95.
9. Schofield R. The trelationship between the spleen colony foming cell and the haematopoietic stem cell. *Blood Cell* 1978;4:7–25.
10. Nilsson SK, Haylock DN, Johnston HM, et al. Hyaluronan is synthesized by primitive hematopoietic cells, participates in their lodgment at the endosteum following transplantation, and is involved in the regulation of their proliferation

and differentiation in vitro. *Blood* 2003;101: 856–62.
11. Zhang J, Niu C, Ye L, et al. Identification of the haematopoietic stem cell niche and control of the niche size. *Nature* 2003;425:836–41.
12. Calvi LM, Adams GB, Weibrecht KW, et al. Osteoblastic cells regulate the haematopoietic stem cell niche. *Nature* 2003;425:841–6.
13. Tavor S, Petit I, Porozov S, et al. CXCR4 regulates migration and development of human acute myelogenous leukemia stem cells in transplanted NOD/SCID mice. *Cancer Res* 2004; 64:2817–24.
14. Jin L, Hope KJ, Zhai Q, et al. Targeting of CD44 eradicates human acute myeloid leukemic stem cells. *Nat Med* 2006;12:1167–74.
15. Avigdor A, Goichberg P, Shivtiel S, et al. CD44 and hyaluronic acid cooperate with SDF-1 in the trafficking of human CD34+ stem/progenitor cells to bone marrow. *Blood* 2004;103:2981–9.
16. Dong JT, Lamb PW, Rinker-Schaeffer CW, et al. KAI1, a metastasis suppressor gene for prostate cancer on human chromosome 11p11.2. *Science* 1995;268:884–86.
17. Ruseva Z, Geiger PX, Hutzler P, et al. Tumor suppressor KAI1 affects integrin alphavbeta3-mediated ovarian cancer cell adhesion, motility, and proliferation. *Exp Cell Res* 2009;315:1759–71.
18. Jee BK, Park KM, Surendran S, et al. KAI1/CD82 suppresses tumor invasion by MMP9 inactivation via TIMP1 up-regulation in the H1299 human lung carcinoma cell line. *Biochem Biophys Res* 2006;342:655–61.
19. Popov C, Radic T, Haasters F, et al. Integrins $\alpha2\beta1$ and $\alpha11\beta1$ regulate the survival of mesenchymal stem cells on collagen I. *Cell Death Dis* 2011;2:e186.
20. Ikezoe T, Yang J, Nishioka C, et al. Inhibition of signal transducer and activator of transcription 5 by the inhibitor of janus kinases stimulates dormant human leukemia CD34(+) /CD38(-) cells and sensitizes them to antileukemia agents. *Int J Cancer* 2011;128:2317–25.
21. Nishioka C, Ikezoe T, Yang J, et al. Long-term exposure of leukemia cells to multi-targeted tyrosine kinase inhibitor induces activations of AKT, ERK and STAT5 signaling via epigenetic silencing of the PTEN gene. *Leukemia* 2010;24: 1631–40.
22. Werb Z, Vu TH, Rinkenberger JL, et al. Matrix-degrading proteases and angiogenesis during development and tumor formation. *APMIS* 1999; 107:11–18.
23. Serada S, Fujimoto M, Ogata A, et al. iTRAQ-based proteomic identification of leucine-rich alpha-2 glycoprotein as a novel inflammatory biomarker in autoimmune diseases. *Ann Rheum Dis* 2010;69:770–4.
24. Ikezoe T, Tanosaki S, Krug U, et al. Insulin-like growth factor binding protein-3 antagonizes the effects of retinoids in myeloid leukemia cells. *Blood* 2004;104:237–42.
25. Ikezoe T, Takeuchi T, Yang J, et al. Analysis of Aurora B kinase in non-Hodgkin lymphoma. *Lab Invest* 2009;89:1364–73.
26. Pearson T, Shultz LD, Miller D, et al. Non-obese diabetic-recombination activating gene-1 (NOD-Rag1 null) interleukin (IL)-2 receptor common gamma chain (IL2r gamma null) null mice: a radioresistant model for human lymphohaematopoietic engraftment. *Clin Exp Immunol* 2008;154:270–84.
27. Unwin RD, Pierce A, Watson RB, et al. Quantitative proteomic analysis using isobaric protein tags enables rapid comparison of changes in transcript and protein levels in transformed cells. *Mol Cell Proteomics* 2005;4:924–35.
28. Ran D, Schubert M, Pietsch L, et al. Aldehyde dehydrogenase activity among primary leukemia cells is associated with stem cell features and correlates with adverse clinical outcomes. *Exp Hematol* 2009;37:1423–34.
29. Gal H, Amariglio N, Trakhtenbrot L, et al. Gene expression profiles of AML derived stem cells; similarity to hematopoietic stem cells. *Leukemia* 2006;20:2147–54.
30. Muranyi AL, Dedhar S, Hogge DE. Targeting integrin linked kinase and FMS-like tyrosine kinase-3 is cytotoxic to acute myeloid leukemia stem cells but spares normal progenitors. *Leuk Res* 2010;34:1358–65.
31. Xie W, Wang X, Du W, et al. Detection of molecular targets on the surface of CD34+ $CD38^-$ bone marrow cells in myelodysplastic syndromes. *Cytometry A.* 2010;77:840–8.
32. Lacraz S, Nicod LP, Chicheportiche R, et al. IL-10 inhibits metalloproteinase and stimulates TIMP-1 production in human mononuclear phagocytes. *J Clin Invest* 1995;96:2304–10.
33. Stearns ME, Fudge K, Garcia F, et al. IL-10 inhibition of human prostate PC-3 ML cell metastases in SCID mice: IL-10 stimulation of TIMP-1 and inhibition of MMP-2/MMP-9 expression. *Invasion Metastasis* 1997;17:62–74.
34. Heissig B, Hattori K, Dias S, et al. Recruitment of stem and progenitor cells from the bone marrow niche requires MMP-9 mediated release of kit-ligand. *Cell* 2002;109:625–37.
35. Pal-Ghosh S, Blanco T, Tadvalkar G, et al. MMP9 cleavage of the $\beta4$ integrin ectodomain leads to recurrent epithelial erosions in mice. *J Cell Sci* 2011;124:2666–75.
36. Iwata S, Kobayashi H, Miyake-Nishijima R, et al. Distinctive signaling pathways through CD82 and beta1 integrins in human T cells. *Eur J Immunol* 2002;32:1328–37.
37. Berditchevski F, Kraeft SK, Chen LB, et al. Transmembrane-4 superfamily proteins CD81 (TAPA-1), CD82, CD63, and CD53 specifically associated with integrin alpha 4 beta 1 (CD49d/ CD29). *J Immunol* 1996;157:2039–47.
38. Matsunaga T, Takemoto N, Sato T, et al. Interaction between leukemic-cell VLA-4 and stromal fibronectin is a decisive factor for minimal residual disease of acute myelogenous leukemia. *Nat Med* 2003;9:1158–65.
39. Papayannopoulou T, Priestley GV, Nakamoto B. Anti-VLA4/VCAM-1-induced mobilization requires cooperative signaling through the kit/ mkit ligand pathway. *Blood* 1998;91:2231–9.
40. Byk T, Kahn J, Kollet O, et al. Cycling G1 CD34+/CD38+ cells potentiate the motility and engraftment of quiescent G0 CD34+/$CD38^-$/low severe combined immunodeficiency repopulating cells. *Stem Cells* 2005;23:561–74.
41. Zheng Y, Sun A, Han ZC. Stem cell factor improves SCID-repopulating activity of human umbilical cord blood-derived hematopoietic stem/ progenitor cells in xenotransplanted NOD/SCID mouse model. *Bone Marrow Transplant* 2005;35: 137–42.
42. Nervi B, Ramirez P, Rettig MP, et al. Chemosensitization of acute myeloid leukemia (AML) following mobilization by the CXCR4 antagonist AMD3100. *Blood* 2009;113:6206–14.
43. Saito Y, Uchida N, Tanaka S, et al. Induction of cell cycle entry eliminates human leukemia stem cells in a mouse model of AML. *Nat Biotechnol* 2010;28:275–80.
44. He B, Liu L, Cook GA, et al. Tetraspanin CD82 attenuates cellular morphogenesis through down-regulating integrin alpha6-mediated cell adhesion. *J Biol Chem* 2005;280:3346–54.
45. Christensen JG, Burrows J, Salgia R. c-Met as a target for human cancer and characterization of inhibitors for therapeutic intervention. *Cancer Lett* 2005;225:1–26.
46. Danilkovitch-Miagkova A, Zbar B. Dysregulation of Met receptor tyrosine kinase activity in invasive tumors. *J Clin Invest* 2002; 109:863–7.
47. Tesio M, Golan K, Corso S, et al. Enhanced c-Met activity promotes G-CSF-induced mobilization of hematopoietic progenitor cells via ROS signaling. *Blood* 2011;117:419–28.
48. Marreiros A, Dudgeon K, Dao V, et al. KAI1 promoter activity is dependent on p53, junB and AP2: evidence for a possible mechanism underlying loss of KAI1 expression in cancer cells. *Oncogene* 2005;24:637–49.
49. Jackson P, Ow K, Yardley G, et al. Expression and clinical significance of p53, JunB and KAI1/ CD82 in human hepatocellular carcinoma. *Hepatobiliary Pancreat Dis Int* 2009;8:389–96.

IJC
International Journal of Cancer

Plasma membrane proteomics identifies bone marrow stromal antigen 2 as a potential therapeutic target in endometrial cancer

Takuhei Yokoyama[1,2], Takayuki Enomoto[1], Satoshi Serada[2], Akiko Morimoto[1,2], Shinya Matsuzaki[1,2], Yutaka Ueda[1], Kiyoshi Yoshino[1], Masami Fujita[1], Satoru Kyo[3], Kota Iwahori[2], Minoru Fujimoto[2], Tadashi Kimura[1] and Tetsuji Naka[2]

[1] Department of Obstetrics and Gynecology, Osaka University Graduate School of Medicine, Osaka, Japan
[2] Laboratory for Immune Signal, National Institute of Biomedical Innovation, Osaka, Japan
[3] Department of Obstetrics and Gynecology, Kanazawa University Graduate School of Medicine, Kanazawa, Japan

This report utilizes a novel proteomic method for discovering potential therapeutic targets in endometrial cancer. We used a biotinylation-based approach for cell-surface protein enrichment combined with isobaric tags for relative and absolute quantitation (iTRAQ) technology using nano liquid chromatography–tandem mass spectrometry analysis to identify specifically overexpressed proteins in endometrial cancer cells compared with normal endometrial cells. We identified a total of 272 proteins, including 11 plasma membrane proteins, whose expression increased more than twofold in at least four of seven endometrial cancer cell lines compared with a normal endometrial cell line. Overexpression of bone marrow stromal antigen 2 (BST2) was detected and the observation was supported by immunohistochemical analysis using clinical samples. The expression of BST2 was more characteristic of 118 endometrial cancer tissues compared with 59 normal endometrial tissues ($p < 0.0001$). The therapeutic effect of an anti-BST2 antibody was studied both *in vitro* and *in vivo*. An anti-BST2 monoclonal antibody showed *in vitro* cytotoxicity in BST2-positive endometrial cancer cells *via* antibody-dependent cell-mediated cytotoxicity and complement-dependent cytotoxicity. In an *in vivo* xenograft model, anti-BST2 antibody treatment significantly inhibited tumor growth of BST2-positive endometrial cancer cells in an NK cell-dependent manner. The anti-BST2 antibody had a potent antitumor effect against endometrial cancer both *in vitro* and *in vivo*, indicating a strong potential for clinical use of anti-BST2 antibody for endometrial cancer treatment. The combination of biotinylation-based enrichment of cell-surface proteins and iTRAQ analysis should be a useful screening method for future discovery of potential therapeutic targets.

Key words: endometrial cancer, molecular target, plasma membrane, iTRAQ, BST2

Abbreviations: ADCC: antibody-dependent cell-mediated cytotoxicity; BST2: bone marrow stromal antigen 2; calcein-AM: calcein-acetoxymethyl ester; CDC: complement-dependent cytotoxicity; E/T ratio: effector to target ratio; FACS: fluorescence activated cell sorting; iTRAQ: isobaric tags for relative and absolute quantitation; LC: liquid chromatography; MS/MS: tandem mass spectrometry; NOD: nonobese diabetic; qRT-PCR: quantitative reverse transcription-PCR; SCID: severe combined immunodeficient; SCX: strong cation exchange; siRNA: small interfering RNA. Additional Supporting Information may be found in the online version of this article.

Grant sponsors: Grant-in-Aid for Scientific Research from the Japanese Ministry of Education, Science, Culture and Sports, Grant-in-Aid from the Ministry of Health, Labour and Welfare of Japan
DOI: 10.1002/ijc.27679
History: Received 5 Mar 2012; Accepted 30 May 2012; Online 22 Jun 2012

Correspondence to: Tetsuji Naka, Laboratory for Immune Signal, National Institute of Biomedical Innovation, 7-6-8 Saitoasagi, Ibaraki City, Osaka 567-0085, Japan, Tel.: +81-72-641-9843, Fax: +81-72-641-9837, E-mail: tnaka@nibio.go.jp

Anticancer monoclonal antibodies are a growing family of novel agents applied in the treatment regimens for hematopoietic and solid tumors. Antibody-based therapeutic agents against CD20 or Her2 have been successfully clinically developed and have significant therapeutic effects.[1,2] Tumor-associated antigens which are easily accessible from the tumor neovasculature are particularly attractive for intravenously-administered antibody-based therapeutic agents. During the last decade, several new technologies for high-throughput screening have identified many potential therapeutic targets. Thus far, no single approach or combination of methods has emerged as the preferred paradigm. It is clear that new tools and strategies are needed so that tumor-associated antigens can be screened efficiently.

Proteomic methods can now be tailored to search directly for targetable cell-surface proteins that distinguish cancer cells from normal cells. The complexity and concentration of individual proteins in the sample are crucial when performing proteomic analyses because abundant proteins, such as cytoskeletal proteins, may hinder the detection of low abundance proteins, such as plasma membrane proteins.[3] One way to enrich the potentially accessible cell-surface proteins is by whole cell protein tagging followed by affinity purification. A method for enrichment of such cell-surface proteins

What's new?
In this study, we have used a biotinylation-based approach for cell-surface protein enrichment combined with iTRAQ technology to identify and quantify membrane proteins which might represent potential therapeutic targets of endometrial cancer. A monoclonal antibody targeting BST2, one of the proteins identified in the iTRAQ analysis, have a potent antitumor effect against endometrial cancer both *in vitro* and *in vivo*, indicating a strong potential for clinical use of anti-BST2 antibody for endometrial cancer treatment.

via their biotinylation and affinity purification has been reported.[4,5] In most cases, concentrated cell-surface proteins are separated by SDS-PAGE and the enzymatically digested peptides are analyzed by mass spectrometry, while highly accurate quantitative data cannot be obtained by using this method. To acquire more quantitative information, stable isotope labeling using amino acids in cell culture (SILAC) based quantitative proteomics has been used, with high quantitative accuracy; however, the SILAC approach has the limitation that only a maximum of three samples can run in any single analysis.[6,7] Compared with SILAC, the more recently developed isobaric tags for relative and absolute quantitation (iTRAQ) technology has a distinct advantage regarding sample number handling capability in a single analysis, because iTRAQ can compare up to eight samples simultaneously.[7,8]

Endometrial cancer is the most common malignant tumor of the female genital tract. Its incidence varies among regions; it is overall the fourth most common malignancy in North America.[9] In general, the prognosis of these patients is excellent as the majority present with early-stage disease that is confined to the uterus at the time of diagnosis, which is followed by simple hysterectomy, leading to a 5-year survival rate of 84%.[9] Unfortunately, those women who present with recurrent or advanced-stage disease have a much poorer prognosis, with a median survival of less than a year.[10] To date, combination chemotherapy of cisplatin, doxorubicin, and paclitaxel has demonstrated the greatest efficacy.[10–12] However, these cytotoxic agents are associated with intolerable side effects and infrequent sustainable remission.[11,12] Thus, new and more effective targeted therapies for endometrial cancer are urgently needed. However, thus far the search for agents effective in the treatment of either recurrent or advanced endometrial cancer has been disappointing.[12]

Aiming for the identification of surface-accessible tumor antigens best suitable for antibody-based therapeutic intervention, it is important to analyze plasma membrane proteins known to be involved in endometrial cancer. For this purpose, we have utilized a novel proteomic technology by combining biotinylation-based approach for cell membrane enrichment and iTRAQ technology using nano liquid chromatography–tandem mass spectrometry (LC-MS/MS) analysis. In this study, one normal endometrial cell line (EM-E6/E7/TERT cells, immortalized normal endometrial cells) and seven endometrial cancer cell lines were used as a comparative model for studying the plasma membrane proteins related to endometrial cancer. Among 272 proteins identified by iTRAQ analysis, bone marrow stromal antigen 2 (BST2) was investigated in more detail. By immunohistochemical analysis using actual clinical specimens, we found that the expression level of BST2 was significantly higher in endometrial cancer tissues compared with normal endometrial tissues. An anti-BST2 antibody showed potent antibody-dependent cell-mediated cytotoxicity (ADCC) and complement-dependent cytotoxicity (CDC) against BST2-positive endometrial cancer cells *in vitro*. In an *in vivo* xenograft model, anti-BST2 antibody treatment significantly inhibited tumor growth.

Taken together, our strategy of screening cell-surface tumor-specific antigens might be useful for identifying new therapeutic targets.

Material and Methods

Cell lines and cultures

We previously established an immortalized normal endometrial cell line (EM-E6/E7/TERT cells).[13,14] Nine human endometrial cancer cell lines (HEC-1, HEC-1A, HEC-6, HEC-88nu, HEC-108, HEC-116, HEC-251, SNG-II, and SNG-M cells) were obtained from the Japanese Collection of Research Bioresources (JCRB, Osaka, Japan), where they were tested and authenticated on June 30, 2011. The method used for testing was multiplexed PCR amplification of eight short tandem repeat loci (TH01, D5S818, D13S317, D7S820, D16S539, CSF1PO, vWA, and TPOX) and amelogenin was performed using the PowerPlex^{TM}16 System (Promega, Madison, WI). PCR-amplified fragments were analyzed with an ABI PRISM 310 Genetic Analyzer (Applied Biosystems, Foster City, CA). Then the fragments were typed based on allelic ladders. EM-E6/E7/TERT cells were maintained in a 1:1 mixture of DMEM and Ham's F12 medium (Wako Pure Chemical Industries, Osaka, Japan) supplemented with 10% FBS (HyClone Laboratories, Logan, UT) and 1% penicillin-streptomycin (Nacalai Tesque, Kyoto, Japan) at 37°C under a humidified atmosphere of 5% CO_2. HEC-1, HEC-1A, HEC-6, HEC-88nu, HEC-108, HEC-116, and HEC-251 cells were maintained and propagated in DMEM (Wako Pure Chemical Industries) supplemented with 10% FBS and 1% penicillin-streptomycin. SNG-II and SNG-M cells were maintained in Ham's F12 (Invitrogen, Carlsbad, CA) with 10% FBS and 1% penicillin-streptomycin.

Biotinylation of bovine serum albumin (BSA)

BSA (30 μM) was biotinylated with a 100-fold molar excess of sulfosuccinimidyl 2-(biotinamido)-ethyl-1,3-dithiopropionate

(sulfo-NHS-SS-biotin; Pierce, Rockford, IL) and desalted as described previously.[15]

Capture of cell-surface proteins

To isolate cell-surface proteins, the normal endometrial cell line (EM-E6/E7/TERT cells) and seven endometrial cancer cell lines (HEC-1, HEC-1A, HEC-6, HEC-108, HEC-116, HEC-251, and SNG-II cells) were grown to approaching confluency (up to 90%) in three 15 cm dishes. Cells were washed three times with prewarmed PBS and then the cell-surface proteins were biotinylated for 15 min at room temperature with 15 ml of 500 μM sulfo-NHS-SS-biotin solution dissolved in PBS. The residual biotinylation reagent was quenched with 5 mM lysine for 5 min at room temperature. After biotinylation, the cells were washed with PBS twice, harvested by scraping, and collected by centrifugation (1,500 rpm, 4°C, 5 min). Detailed methods of extraction and purification of biotinylated cell-surface proteins are described in the Supporting Information Materials and Methods section.

iTRAQ labeling

Trypsin-digested peptides were dissolved in 5 μl of 9.8 M urea and 20 μl of 1M TEAB. Samples were labeled with the iTRAQ reagent according to the manufacturer's protocol (Applied Biosystems). EM-E6/E7/TERT cells were labeled with iTRAQ reagent 113, HEC-1 cells with 114, HEC-1A cells with 115, HEC-6 cells with 116, HEC-108 cells with 117, HEC-116 cells with 118, HEC-251 cells with 119, and SNG-II cells with 121. The labeled peptide samples were then pooled and desalted with Sep-Pak Light C18 Cartridges (Waters, Manchester, UK) and peptides were dried in a centrifugal concentrator (Micro Vac MV-100, Tomy, Tokyo, Japan) before strong cation exchange (SCX) fractionation.

SCX fractionation

In order to remove excess unreacted iTRAQ reagent and to simplify the complexity of the peptide mixture, the labeled peptide mixtures were purified and fractionated using SCX column (SCX, PolySulfoethyl A column, 2.1 × 150 mm, 5 μm, 300 Å) on an Agilent 1200 HPLC system. Detailed information is provided in the Supporting Information Materials and Methods section.

Mass spectrometric analysis

Nano LC-MS/MS analyses were performed on an LTQ-Orbitrap XL (Thermo Fisher Scientific, Waltham, MA) equipped with a nano-ESI source and coupled to a Paradigm MG4 pump (Michrom Bioresources, Auburn, CA) and autosampler (HTC PAL, CTC Analytics, Zwingen, Switzerland). Detailed information is provided in the Supporting Information Materials and Methods section.

iTRAQ data analysis

Protein identification and quantification for iTRAQ analysis was carried out using Proteome Discoverer software (v. 1.1) (Thermo Fisher Scientific) against Swiss Prot human protein database (SwissProt_2011_11, 533,049 entries). Taxonomy was set to *Homo sapiens* (20,326 entries) or mammalian (65,656 entries). Search parameters for peptide and MS/MS mass tolerance were 10 ppm and 0.8 Da, respectively, with allowance for two missed cleavages made from the trypsin digest. Carbamidomethylation (Cys) and iTRAQ8plex (Lys, N-terminal) were specified as static modifications, whereas CAMthiopropanoyl (Lys, N-terminal), iTRAQ8plex (Tyr), and oxidation (Met) were specified as variable modifications in the database search. The false discovery rate of 1% was calculated by Proteome Discoverer based on a search against a corresponding randomized database. Relative protein abundances were calculated using the ratio of iTRAQ reporter ion in the MS/MS scan. For subcellular localization, all the proteins identified in this analysis were analyzed using the UniprotKB (available at: http://www.uniprot.org/) and Ingenuity Pathway Analysis software (Ingenuity Systems, Redwood City, CA).

Quantitative reverse transcription-PCR (qRT-PCR) analysis

To confirm the altered expression of BST2 in endometrial cancer, the normal endometrial cell line (EM-E6/E7/TERT cells) and nine endometrial cancer cell lines (HEC-1, HEC-1A, HEC-6, HEC-88nu, HEC-108, HEC-116, HEC-251, SNG-II, and SNG-M cells) were subjected to qRT-PCR. Total RNA was extracted using an RNeasy Mini Kit (Qiagen, Valencia, CA) and cDNAs were synthesized with a QuantiTect Reverse Transcription Kit (Qiagen), all according to the manufacturers' instructions. qRT-PCR was performed using SYBR Premix Ex taq (Takara Bio, Shiga, Japan) and an ABI 7900HT real-time PCR instrument (Applied Biosystems). β-Actin was used as a housekeeping gene for normalization of quantitative real-time PCR analysis. The primer sequences and the expected sizes of PCR products were as follows: BST2, forward primer 5′-GGAGGAGCTTGAGGGAGAG-3′ and reverse primer 5′-CTCAGTCGCTCCACCTCTG-3′, 75 bp; β-actin, forward primer 5′-AGCCTCGCCTTTGCCGA-3′ and reverse primer 5′-CTGGTGCCTGGGGCG-3′, 174 bp. Relative quantitation of gene expression was performed using the standard curve method as outlined by Applied Biosystems. Experimental conditions were tested in triplicate and three independent experiments were performed.

Fluorescence activated cell sorting (FACS) analysis

Cells were washed twice in PBS (Nacalai Tesque) and detached with 0.02% EDTA solution (Nacalai Tesque). Cells were washed twice with cold FACS buffer (PBS supplemented with 1% FBS and 0.1% sodium azide) and then incubated with mouse anti-human BST2 antibody (Biolegend, San Diego, CA) at a 1:100 dilution and labeled with Alexa Fluor 488-labeled donkey anti-mouse IgG antibody (Invitrogen). Stained cells were analyzed using a FACS Canto cytometer (Becton Dickinson, Mountain View, CA) and the results were analyzed using FlowJo software (Tree Star, Stanford, CA).

Patients and tissue samples

The formalin-fixed, paraffin-embedded tissue sections of 59 cases of normal endometrium and 118 cases of endometrial cancer were obtained from 177 patients who underwent surgical resections at Osaka University Hospital, Japan, between 1998 and 2007. Cases of normal endometrium were obtained from 59 patients who underwent simple hysterectomy for benign indications such as leiomyoma and uterine prolapse. Histological features of the tissues were reviewed by board-certified pathologists. The degree of histological differentiation and surgical pathological staging of 118 cases of endometrial cancer were assigned according to the 1988 recommendations of International Federation of Gynecology and Obstetrics. A summary of clinicopathological information for these patients is shown in Supporting Information Table S1. Written informed consent was obtained for all the cases and the experimental protocol was approved by the ethics committees of Osaka University and National Institute of Biomedical Innovation.

Immunohistochemistry

Sections were prepared from formalin-fixed, paraffin-embedded tissue specimens, deparaffinized, and rehydrated in graded alcohols. Immunohistochemical staining for BST2 was performed using the avidin-biotin-peroxidase complex (ABC) method using a rabbit polyclonal anti-BST2 antibody (Sigma-Aldrich, St. Louis, MO) and the Vectastain ABC kit (Vector Laboratories, Burlingame, CA) according to the manufacturer's protocol. Immunostained sections were photographed with an Olympus FSX100 (Olympus, Tokyo, Japan). Detailed information is provided in the Supporting Information Materials and Methods section.

Evaluation of immunohistostaining

Immunostainings were scored according to the intensity of the staining (no staining = 0, weak staining = 1, moderate staining = 2, strong staining = 3) and the extent of stained cells (0–9% = 0, 10–40% = 1, 41–70% = 2, 71–100% = 3). The final immunohistochemistry (IHC) score was determined by multiplying the intensity score (0, 1, 2, or 3) with the positivity score (0, 1, 2, or 3), resulting in a maximum score of 9. Three independent gynecologic oncologists (Y.U., K.Y., and M.F.), blinded to the histological data, analyzed the stained sections using an Olympus BH2 microscope (Olympus). In case of disagreement, the staining results were re-evaluated by careful discussion until a consensus was reached.

Cell proliferation assay

Endometrial cancer cells plated in 96-well plates (1,000 cells per well) were grown in their respective media for 24, 48, or 72 hr after the addition of antibody or small interfering RNA (siRNA) transfection. At each time point, cell proliferation was assessed by a WST-8 assay according to the manufacturer's protocol (Nacalai Tesque). Detailed information for these assays can be found in the Supporting Information Materials and Methods section.

ADCC assay

ADCC was measured by calcein-acetoxymethyl ester (calcein-AM) release assay, with sensitivity similar to the traditional ^{51}Cr release assay.[16,17] Detailed information for this assay can be found in the Supporting Information Materials and Methods section.

CDC assay

CDC was evaluated using a ^{51}Cr release assay.[18] Detailed information for this assay can be found in the Supporting Information and Methods section.

Tumor xenograft and antibody therapy

Healthy female severe combined immunodeficient (SCID) and nonobese diabetic (NOD)/SCID mice at 8 weeks of age were obtained from Charles River Japan (Yokohama, Japan) and maintained in a specific pathogen-free facility. For subcutaneous xenograft experiments, SCID mice were inoculated subcutaneously with 5×10^6 HEC-88nu or SNG-II cells in a total volume of 50 μl of 1/1 (v/v) PBS/Matrigel (Becton Dickinson) into the abdomen. NOD/SCID mice were inoculated with 5×10^6 HEC-88nu cells. PBS, isotype control (mouse IgG2aκ, Sigma-Aldrich), or mouse anti-human BST2 antibody (clone 1B4: Chugai Pharmaceutical) was administered intraperitoneally at a dose of 5 mg/kg (SNG-II) or 10 mg/kg (HEC-88nu) in 400 μl of PBS. Six mice were used per group. The first dose was given on day 4 (SNG-II) or 9 (HEC-88nu) and continued twice weekly for 4 weeks. Tumors were measured twice weekly from days 4 (SNG-II) or 9 (HEC-88nu) using vernier calipers throughout the study. Tumor volumes were calculated using the following formula: tumor volume (mm^3) = length × width × height. After 8 (HEC-88nu) or 12 (SNG-II) weeks, tumors were resected and weighted. All animal experiments were conducted according to the institutional ethical guidelines for animal experimentation of the National Institute of Biomedical Innovation.

Statistical analysis

For immunohistochemistry, statistical significance of difference between normal endometrium and endometrial cancer was analyzed by the nonparametric Mann–Whitney *U* test. Differences in the *in vitro* cytotoxic assay were determined by using the Kruskal–Wallis test followed by the Steel procedure. For all subcutaneous tumor comparisons, groups were analyzed using the Kruskal–Wallis test followed by the Steel-Dwass procedure.

Results

Protein expression profiles in normal endometrium and endometrial cancer

To identify potential therapeutic targets of endometrial cancer, we performed comparative protein expression profiling between normal endometrium (EM-E6/E7/TERT cells) and

endometrial cancer (HEC-1, HEC-1A, HEC-6, HEC-108, HEC-116, HEC-251, and SNG-II cells) at the cell surface level. We identified a total of 272 proteins by a biotinylation-based approach for cell membrane enrichment combined with iTRAQ technology using nano LC-MS/MS analysis. The complete list of all the proteins identified is shown in Supporting Information Table S2. The list of proteins identified with single peptide is provided in Supporting Information Table S3. MS/MS spectra of all single-peptide-based assignments with masses detected as well as fragment assignments are presented in Supporting Information Table S4. The raw MS data of this analysis is publicly available for download from PeptideAtlas (available at: http://www.peptideatlas.org/PASS/PASS00032). To correct the error of quantitation during chromatographic procedures, we added the equivalent moles of the sulfo-NHS-SS-biotin labeled BSA into the each sample as an internal standard. The iTRAQ ratio of BSA (0.873 to 1.131, Supporting Information Table S3) was used for the correction of quantitation information accurately. According to the annotation from UniprotKB and Ingenuity Pathway Analysis, 139 proteins (51% of the identified proteins) were located in the plasma membrane (Fig. 1*a*). Among these 139 plasma membrane proteins identified, 11 proteins were increased more than twofold in at least four of seven endometrial cancer cell lines compared with the normal endometrial cell line (Table 1). As expected, neural cell adhesion molecule L1, a plasma membrane protein previously known to be overexpressed in endometrial cancer, was identified again. Interestingly, BST2 was found to show one of the most significant differences in expression between normal endometrial cells and endometrial cancer cells, making it a prime target.

Confirmatory studies by qRT-PCR and FACS

To confirm the altered expression of BST2 in endometrial cancer, we first evaluated its transcripts by qRT-PCR in the normal endometrial cell line (EM-E6/E7/TERT cells) and nine endometrial cancer cell lines (HEC-1, HEC-1A, HEC-6, HEC-88nu, HEC-108, HEC-116, HEC-251, SNG-II, and SNG-M cells). BST2 mRNA expression was clearly detected in seven of the nine endometrial cancer cell lines, while the normal endometrial cell line showed no detectable expression of BST2 transcripts (Fig. 1*b*).

We then evaluated the expression of BST2 at the protein level and confirmed the surface localization of BST2 by FACS analysis. Protein expression of BST2 was very weak in EM-E6/E7/TERT cells. In contrast, a considerably higher level of BST2 protein expression was detected in six of the nine endometrial cancer cell lines on the cell surface (Fig. 1*c*). Together our data demonstrate that BST2 was overexpressed in endometrial cancer cells at both the mRNA and protein level; this was consistent with our iTRAQ analysis.

Validation study by IHC

As a validation study, immunohistochemical analyses were performed by examination of the BST2 expression pattern in paraffin-embedded tissue samples (Supporting Information Table S1). Representative immunohistochemical staining of BST2 in tissue sections from patients revealed intense BST2 staining in endometrial cancer compared with normal endometrium (Fig. 2*a*). In addition, immunohistochemical analyses showed membranous immunoreactivity in endometrial cancer cells, indicating that the localization of BST2 was at cell surface. We observed significantly stronger positive staining of BST2 in tissue sections from patients with endometrial cancer compared with normal endometrium ($p < 0.0001$) (Fig. 2*b*). In 118 endometrial cancer specimens, moderately to strongly positive staining (IHC score = 3–9) was detected in 71.2% of specimens (84 of 118), whereas only 1.7% (1 of 59) were positive in the normal endometrial specimens. There were no significant differences in BST2 immunohistochemical staining among endometrial cancer tissues according to their degree of histological differentiation or surgical pathological staging ($p = 0.77$ and 0.06, respectively, by the Kruskal–Wallis test). There were no significant differences in BST2 staining among normal proliferative-phase, secretory-phase, and atrophic endometrium ($p = 0.82$ by the Kruskal–Wallis test). These results indicate that BST2 was overexpressed on the cell surface of endometrial cancer tissues much more frequently than in normal endometrium, raising the possibility that BST2 might represent a potential therapeutic target.

BST2-siRNA and anti-BST2 antibody treatment *in vitro*

To examine whether the BST2 expression contributes to cell proliferation of endometrial cancer cells, the effect of BST2-siRNA treatment in four of the endometrial cancer cell lines expressing BST2 (HEC-6, HEC-88nu, HEC-116, and SNG-II cells) was evaluated using the WST-8 assay. To ensure silencing efficiency, BST2 expression was analyzed by FACS analysis after 48 hr of siRNA transfection. The two siRNAs targeting BST2 (Hs_BST2_1 and Hs_BST2_5) had a similar silencing effect on the protein level (Supporting Information Fig. S1). There were no significant differences in cell proliferation among BST2-siRNA and control-siRNA treated cells (Fig. 3*a*). Similarly, anti-BST2 antibody treatment did not affect *in vitro* cell proliferation (Fig. 3*b*).

We subsequently examined whether an anti-BST2 antibody can induce ADCC among endometrial cancer cells using the calcein-AM release assay. To study the specificity of anti-BST2 antibody-mediated ADCC against BST2-expressing target cells, an ADCC assay was performed using a BST2-expressing endometrial cancer cell line (HEC-88nu cells) and a BST2-negative cell line (HEC-1 cells). As shown in Figure 3*c*, HEC-88nu cells treated with the anti-BST2 antibody showed specific lysis *via* ADCC ($p = 0.045$), whereas the anti-BST2 antibody showed no lytic activity against HEC-1 cells.

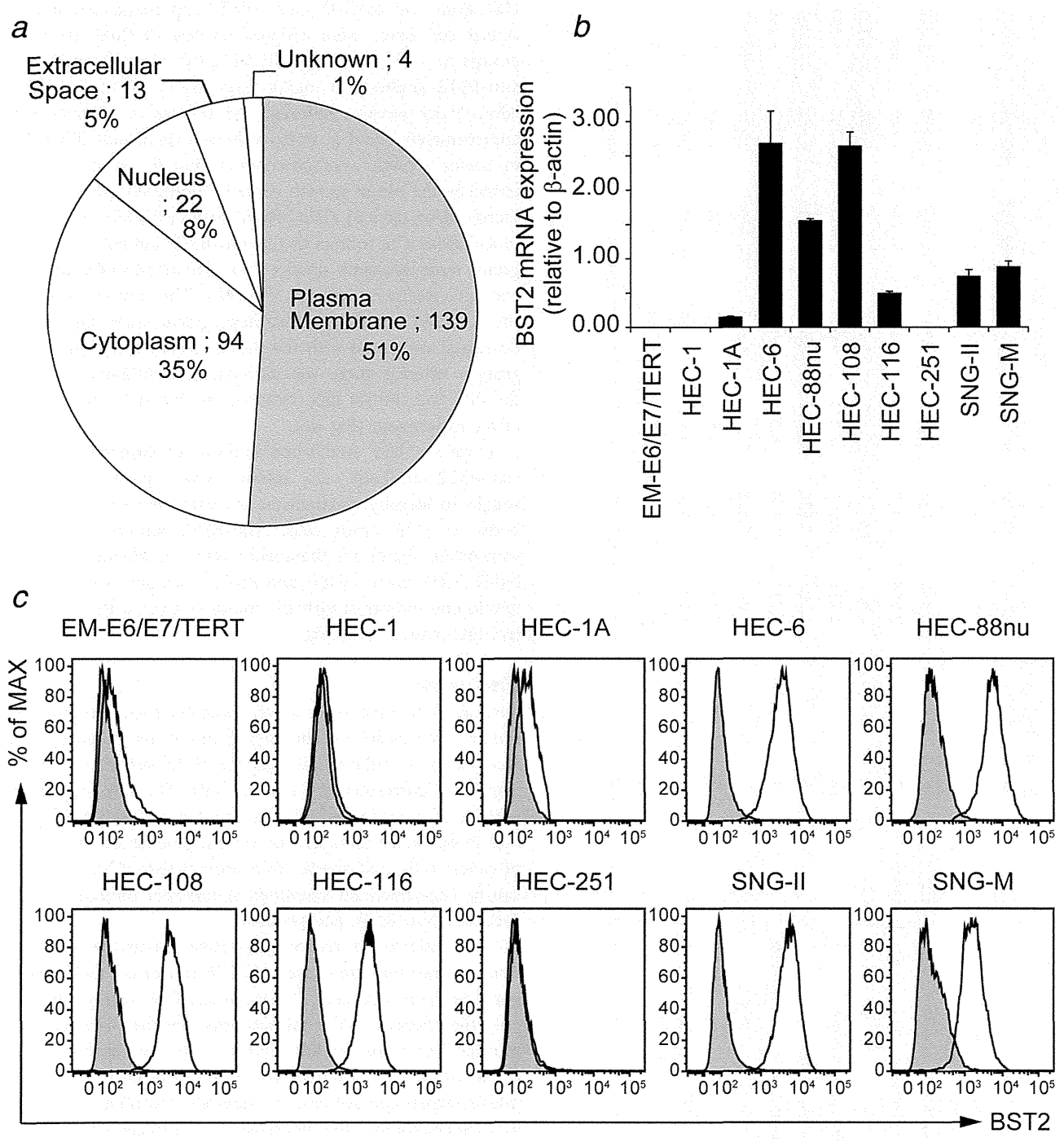

Figure 1. (*a*) Subcellular localization of the identified 272 proteins analyzed by UniprotKB and Ingenuity Pathway Analysis. (*b*) Confirmation of iTRAQ results by qRT-PCR. qRT-PCR was used to quantify BST2 mRNA; β-actin was used as the internal control. Data are mean ± SEM of three independent experiments, each performed in triplicate. BST2 mRNA expression was not detected in the normal endometrial cell line (EM-E6/E7/TERT cells), but seven of nine endometrial cancer cell lines exhibited positive expression of BST2 mRNA. (*c*) Confirmation of iTRAQ results by FACS analysis. The shaded histogram profile indicates the isotype control, and the open histogram indicates the anti-BST2 antibody staining results.

We also examined CDC exhibited by the anti-BST2 antibody. Figure 3*d* shows that the BST2-expressing endometrial cancer cell line (HEC-88nu cells), but not the BST2-negative cell line (HEC-1 cells), was sensitive to CDC ($p = 0.045$).

Therapeutic effect of the anti-BST2 antibody *in vivo*

To evaluate the therapeutic efficacy of anti-BST2 antibody therapy, *in vivo* studies were performed using an endometrial cancer xenograft model. SCID mice injected with either

Table 1. Plasma membrane proteins overexpressed in endometrial cancer cells

Accession number	Protein name	No. peptides used for identification	iTRAQ ratio						
			HEC-1	HEC-1A	HEC-6	HEC-108	HEC-116	HEC-251	SNG-II
O14672	Disintegrin and metalloproteinase domain-containing protein 10	5	1.670	1.271	2.032	3.175	2.824	3.958	1.364
P11279	Lysosome-associated membrane glycoprotein 1	1	0.398	3.017	5.745	8.722	4.307	5.239	1.727
P25942	Tumor necrosis factor receptor superfamily member 5	2	2.518	5.353	7.796	6.438	8.526	2.747	n.d.
P31431	Syndecan-4	5	n.d.	n.d.	0.949	11.644	2.905	4.396	8.121
P32004	Neural cell adhesion molecule L1	26	1.211	0.905	2.171	9.025	2.603	13.756	4.283
P50895	Basal cell adhesion molecule	15	0.692	0.876	5.378	2.493	2.363	3.936	2.864
P78310	Coxsackievirus and adenovirus receptor	3	1.773	3.140	5.228	16.042	4.507	3.265	3.256
Q10589	Bone marrow stromal antigen 2	2	n.d.	6.438	85.276	94.318	87.278	3.435	38.946
Q14126	Desmoglein-2	9	2.360	3.199	1.912	2.827	5.286	2.542	4.637
Q9H5V8	CUB domain-containing protein 1	2	0.907	2.234	11.680	3.508	11.603	8.623	17.020
Q9Y624	Junctional adhesion molecule A	1	4.374	17.088	25.645	47.784	23.673	77.025	18.523

The iTRAQ ratios were calculated comparing the endometrial cancer cells' iTRAQ signal divided by the normal endometrial cells' iTRAQ signal. Proteins overexpressed more than twofold in at least four cell lines are listed.
Abbreviations: n.d. = Not detected.

HEC-88nu or SNG-II cells (BST2-expressing endometrial cancer cell lines) were assigned to one of three treatment groups ($n = 6$ per group): (*i*) PBS; (*ii*) isotype control; (*iii*) anti-BST2 antibody, 5 mg/kg (SNG-II) or 10 mg/kg (HEC-88nu) twice weekly. Although the tumors of all mice were approximately equal in initial volumes, significant differences in tumor growth were observed during the study, as illustrated by the tumor growth curve in Figure 4*a*. All mice were sacrificed on days 61 (HEC-88nu) or 85 (SNG-II) post-tumor inoculation. The tumors of the anti-BST2 antibody treatment group were markedly smaller than that of the PBS and control IgG treatment groups (Fig. 4*b*). The tumor weights of the anti-BST2 antibody treatment group were significantly decreased compared with the PBS and control IgG treatment groups, whereas there was no statistical difference between the PBS and control IgG treatment groups at the termination of the experiment (Fig. 4*c*).

Once we had established a proof of principle that the anti-BST2 antibody can inhibit tumor growth, we then sought to identify mechanisms by which the anti-BST2 antibody acts on tumor cells. Anti-BST2 antibody treatment showed no significant therapeutic effect in identically treated NOD/SCID mice, with anti-BST2 antibody treated mice developing tumors at virtually the same rate as PBS and control IgG treated mice (Fig. 5).

Discussion

Our study focused on a novel biotechnological method we found to be useful for identifying tumor-associated cell-surface antigens differentially expressed in cancer cells with respect to corresponding normal cells. The ideal expression pattern of a tumor-specific antigen for antibody therapy is that it should be abundant and homogeneous on the surface of cancer cells, and absent from normal tissue.[19] Such targets can be experimentally identified at different molecular levels, such as DNA, RNA, and protein.

DNA microarray technologies have led to the identification of genes that are dysregulated in cancer cells when compared with normal cells.[20,21] However, DNA arrays measure only the changes at the mRNA level, and this is not always translated to corresponding changes at the protein level, leading to many false positives and missed positives. The use of mRNA expression patterns by themselves is often insufficient for understanding the expression of protein products, as additional post-translational mechanisms, including protein translation, post-translational modification, and degradation, may influence the level of a protein and its antigenic epitopes.[22,23] In addition, effective induction of ADCC or CDC mediated by a therapeutic antibody requires abundant expression of cell-surface proteins specifically on the cancer cells,[24,25] providing a compelling rationale for a more direct analysis of gene expression at the protein level by proteomic methods.

The intensity of individual proteins in the sample is crucial when performing proteomic analyses, as larger amounts

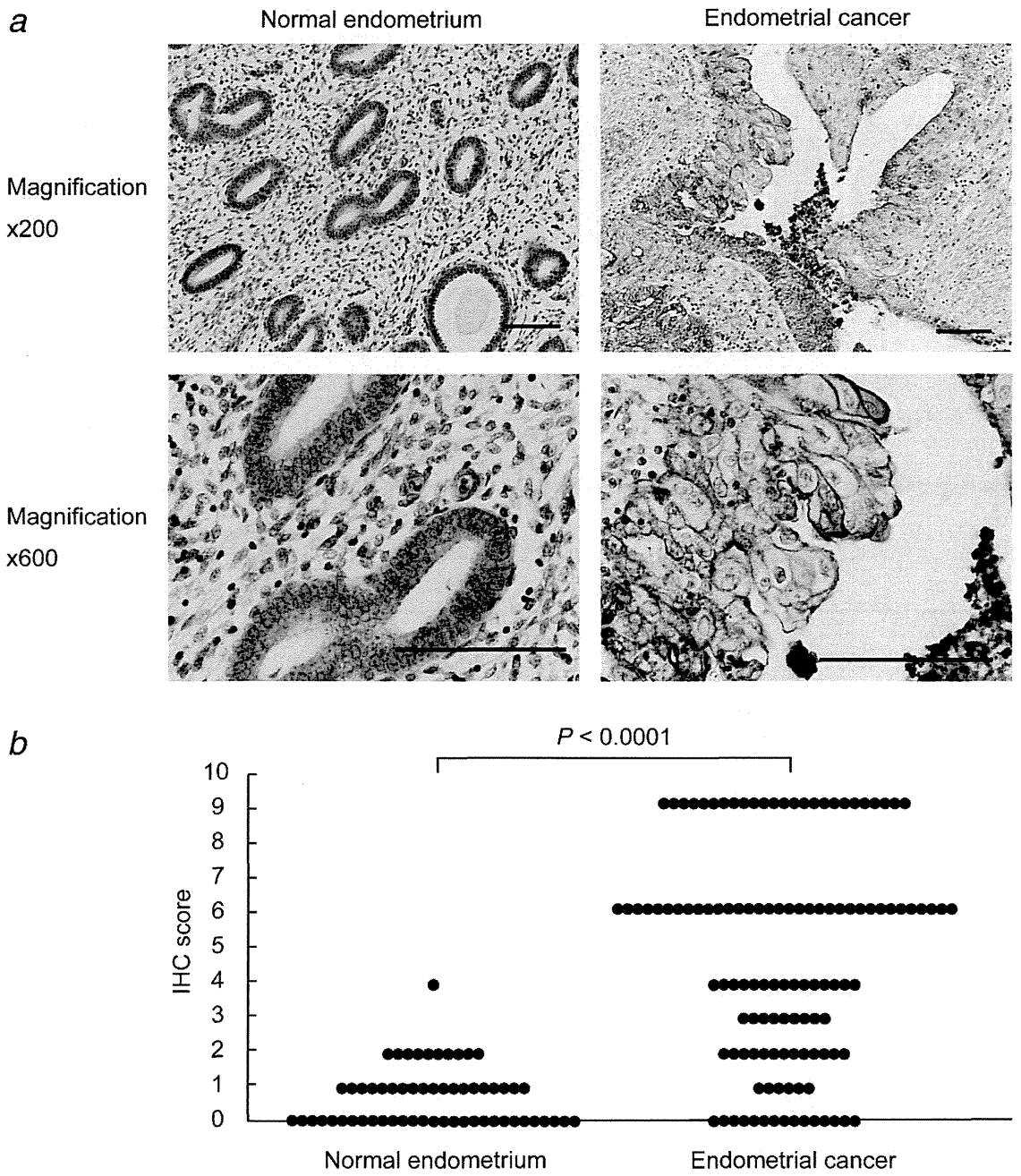

Figure 2. (*a*) Representative immunohistochemical staining for BST2 in normal endometrium and endometrial cancer specimens. Immunostained sections were counterstained with hematoxylin and photographed with an Olympus FSX100 (Olympus). The expression of BST2 was negative in normal endometrium, whereas endometrial cancer showed strong membranous reactivity for BST2. Scale bar, 100 μm. (*b*) BST2 immunoreactivity in normal endometrial tissues and endometrial cancer tissues. The expression of BST2 was increased in endometrial cancer, with significant difference ($p < 0.0001$). IHC score = intensity score (0, 1, 2, or 3) × positivity score (0, 1, 2, or 3).

of some proteins may hinder the detection of less abundant proteins, such as cell-surface membrane proteins. As such, enrichment of plasma membrane proteins is an important initial step. Physical isolation of membrane proteins using centrifugation and/or chemical extraction are well-described methods.[26,27] However, these techniques fail to isolate only the cell-surface membrane proteins and usually provide extracts that consist of all the membrane structures, including those inside the cell (e.g., endoplasmic reticulum, Golgi apparatus, and mitochondrial membranes). The proteins that are found inside the cell will most likely not be accessible to the systemically delivered antibodies and hence do not represent a group of interest for discovery of targetable molecules. Another way to enrich specifically the potentially accessible

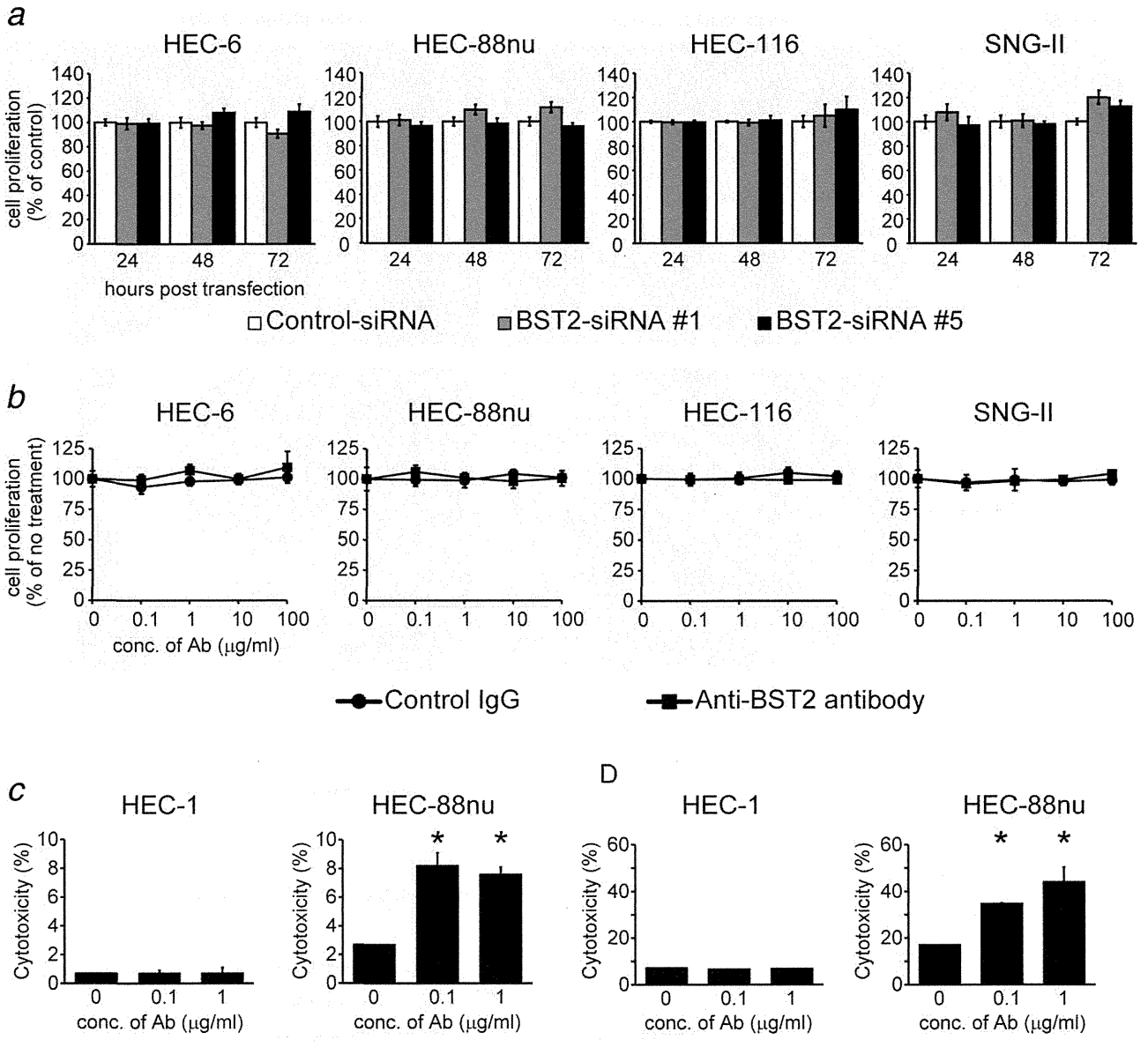

Figure 3. *In vitro* growth assay of endometrial cancer cells treated with BST2-siRNA (*a*) or anti-BST2 antibody (*b*). HEC-6, HEC-88nu, HEC-116, and SNG-II cells are BST2-positive endometrial cancer cell lines. (*a*) A total of 1,000 cells were plated in each well of 96-well plates and then siRNA was transfected. Cell proliferation was assessed at 24, 48, and 72 hr using a WST-8 assay. Values were normalized to control-siRNA treated cells. There were no significant differences in cell proliferation among BST2-siRNA and control-siRNA treated cells. (*b*) Anti-BST2 antibody or isotype-control IgG (final concentrations of 0.1, 1, 10, or 100 μg/ml) were added to 1,000 cells/well in 96-well plates. Cell proliferation was assessed at 72 hr using the WST-8 assay. Values were normalized to untreated cells. Anti-BST2 antibody had no direct cytotoxic effect on endometrial cancer cells *in vitro*. (*c*), ADCC activity of anti-BST2 antibody. Calcein-labeled HEC-1 (BST2-negative) and HEC-88nu (BST2-positive) cells were incubated with bone marrow-derived lymphokine-activated killer cells at an *E/T* ratio of 50 in the presence of 0, 0.1, or 1.0 μg/ml anti-BST2 antibody. (*d*) CDC activity of anti-BST2 antibody. ^{51}Cr-labeled HEC-1 (BST2-negative) and HEC-88nu (BST2-positive) cells were incubated with 12.5% baby rabbit complement in the presence of 0, 0.1, or 1.0 μg/ml anti-BST2 antibody. Anti-BST2 antibody had ADCC and CDC activity against HEC-88nu cells (BST2-expressing endometrial cancer cell line). *$p = 0.045$.

cell-surface proteins involves conjugating membrane proteins with the small molecule biotin and using the receptor streptavidin to extract the labeled proteins.[28,29]

In this study, we quantitatively analyzed the plasma membrane profiles comparing normal endometrium and endometrial cancer using a biotinylation-based approach for cell membrane enrichment combined with iTRAQ technology using nano LC-MS/MS analysis. While quantitative membrane proteomic approaches combining biotin labeling followed by enrichment of cell surface membrane proteins by avidin-beads and SILAC technology or spectral counting were already reported,[28,30] we demonstrated that iTRAQ approach is also an alternative method, suitable for the quantitative analysis of the cell surface membrane proteins.

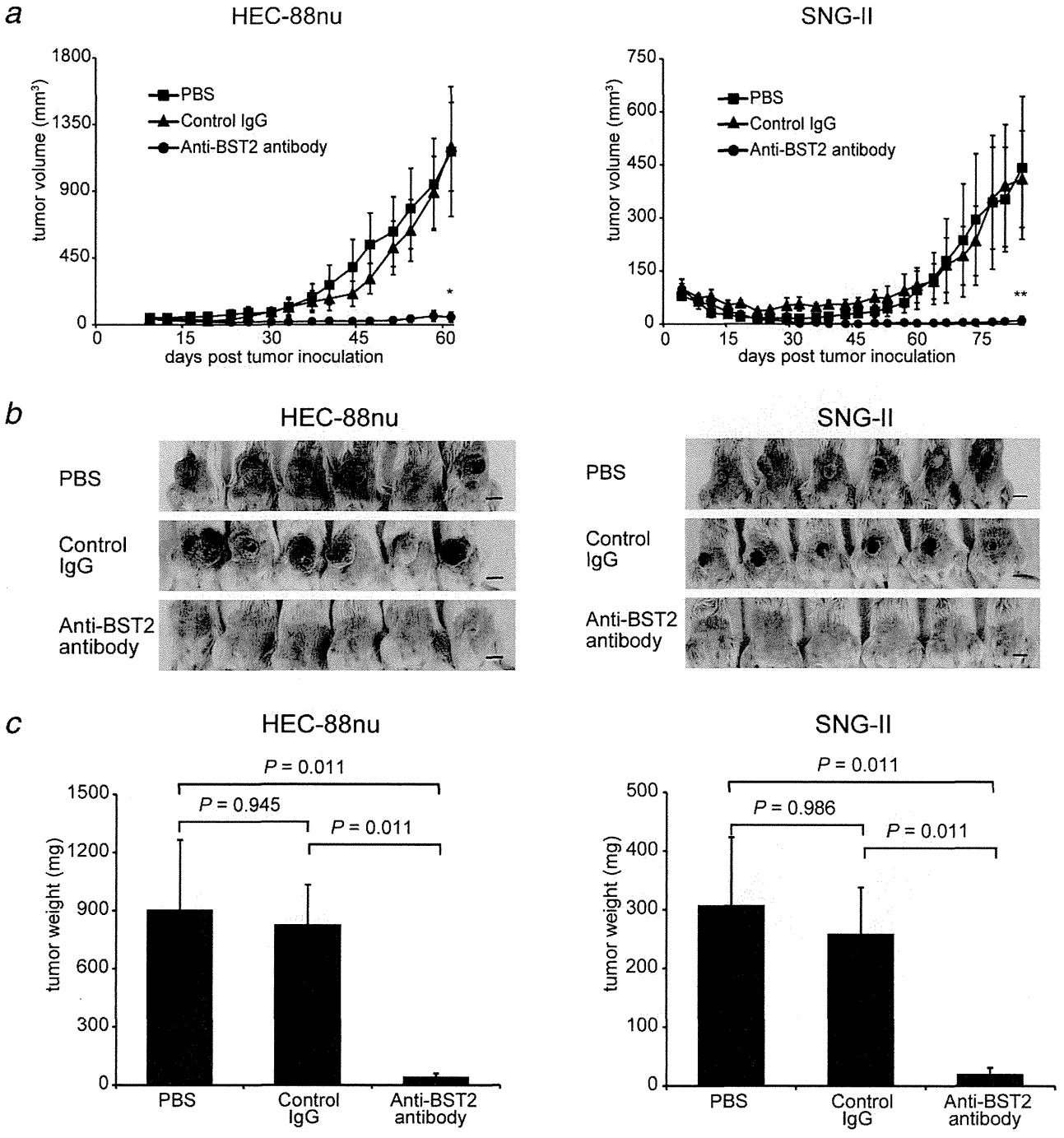

Figure 4. *In vivo* therapeutic effect of anti-BST2 antibody on endometrial cancer growth. SCID mice inoculated with HEC-88nu or SNG-II cells (both are BST2-expressing endometrial cancer cell lines) received PBS, control IgG, or anti-BST2 antibody twice a week for 4 weeks from days 4 (SNG-II) or 9 (HEC-88nu) post-tumor inoculation. (*a*) Time-course of tumor volume change. Tumor volumes were measured twice a week and calculated as the product of length, width, and height. The mean volume ± SD of six tumors in each group is shown. Anti-BST2 antibody treatment resulted in significantly decreased tumor growth compared with the other control groups (PBS and control IgG) at the termination of the experiment. *$p = 0.0110$, **$p = 0.0108$. (*b*) Mice at the end of the experiment. Scale bar, 1 cm. (*c*) Tumor weight at autopsy. After 4 (HEC-88nu) or 8 (SNG-II) weeks of observation following treatment, tumors were removed and weighted. Their weights were significantly different between the experimental (anti-BST2 antibody) group and the control (PBS and control IgG) groups ($p = 0.011$).

In total, we identified 272 proteins, 139 of which (51%) were found to be cell-surface proteins. Given that global genomic analysis predicts that 20 to 30% of all open reading frames encode integral membrane proteins,[31] our results indicate that the membrane proteins were moderately enriched by our sample preparation strategy.